iScience

CellPress
OPEN ACCESS

Article

Tandem detergent-extraction and immunoprecipitation of proteinopathy: Scalable enrichment of ALS-associated TDP-43 aggregates

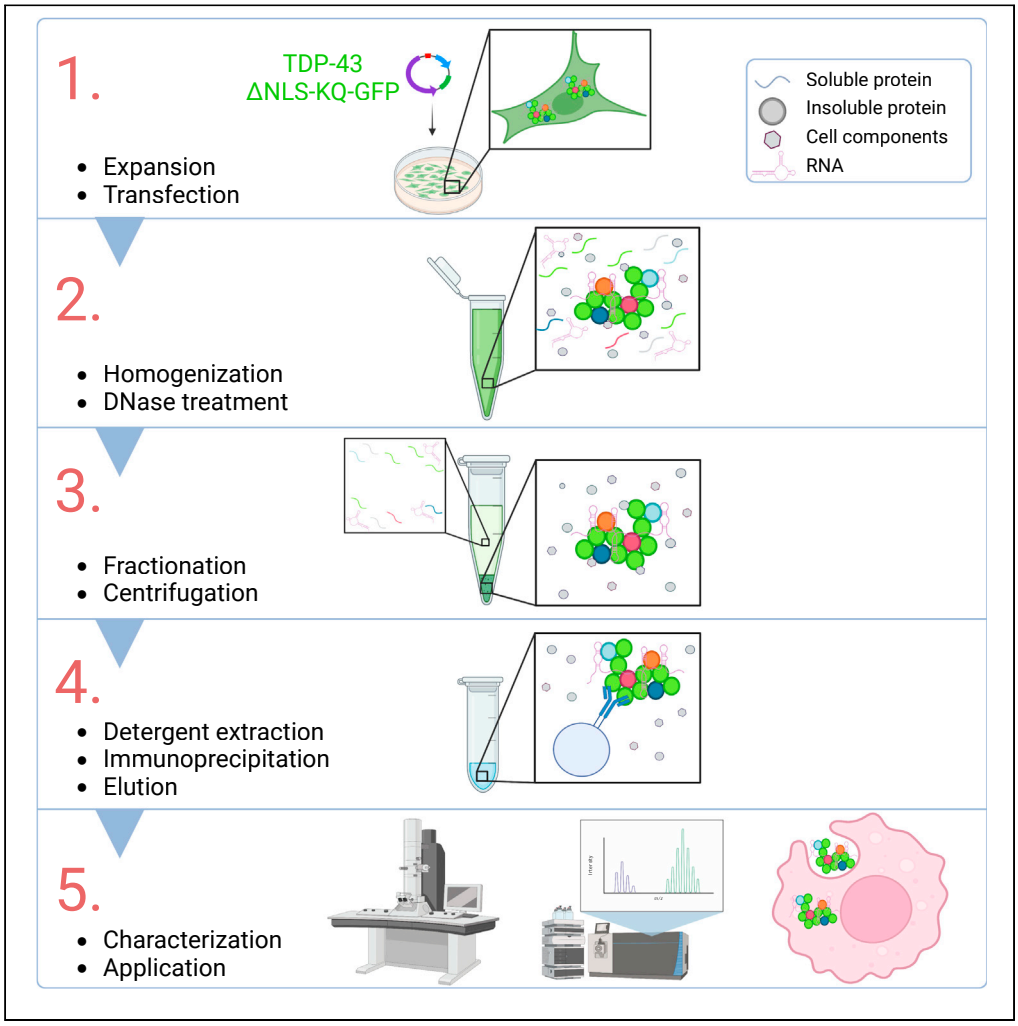

Baggio A. Evangelista, Shannon R. Cahalan, Joey V. Ragusa, ..., Rick Meeker, Laura E. Herring, Todd J. Cohen

toddcohen@neurology.unc.edu

Highlights

TDiP offers scalable purification of TDP-43 aggregates formed *in situ*

TDiP aggregates recapitulate the pathological features of human ALS pathology

TDiP aggregates harbor a diverse proteome and seed endogenous TDP-43

TDiP aggregates are suitable for live-cell interaction and trafficking studies

Evangelista et al., iScience *26*, 106645
May 19, 2023 © 2023 The Author(s).
https://doi.org/10.1016/j.isci.2023.106645

iScience

CellPress
OPEN ACCESS

Article

Tandem detergent-extraction and immunoprecipitation of proteinopathy: Scalable enrichment of ALS-associated TDP-43 aggregates

Baggio A. Evangelista,[1] Shannon R. Cahalan,[2] Joey V. Ragusa,[1] Angie Mordant,[3] Julie C. Necarsulmer,[1] Robert J. Perna,[4] Tejazaditya Ajit,[4] Kristen White,[5] Natalie K. Barker,[3] Xu Tian,[4] Sarah Cohen,[1] Rick Meeker,[4] Laura E. Herring,[3] and Todd J. Cohen[1,4,6,7,8,*]

SUMMARY

Transactive response DNA-binding protein of 43 kDa (TDP-43) is a highly conserved, ubiquitously expressed nucleic acid-binding protein that regulates DNA/RNA metabolism. Genetics and neuropathology studies have linked TDP-43 to several neuromuscular and neurological disorders including amyotrophic lateral sclerosis (ALS) and frontotemporal lobar degeneration (FTLD). Under pathological conditions, TDP-43 mislocalizes to the cytoplasm where it forms insoluble, hyper-phosphorylated aggregates during disease progression. Here, we optimized a scalable *in vitro* immuno-purification strategy referred to as tandem detergent-extraction and immunoprecipitation of proteinopathy (TDiP) to isolate TDP-43 aggregates that recapitulate those identified in postmortem ALS tissue. Moreover, we demonstrate that these purified aggregates can be utilized in biochemical, proteomics, and live-cell assays. This platform offers a rapid, accessible, and streamlined approach to study ALS disease mechanisms, while overcoming many limitations that have hampered TDP-43 disease modeling and therapeutic drug discovery efforts.

INTRODUCTION

Transactive response DNA binding protein of 43 kDa (TDP-43) is a highly conserved nucleic acid-binding protein necessary for DNA/RNA regulation.[1–4] Structurally, TDP-43 contains two RNA recognition motifs (RRM1 and RRM2) that facilitate protein-nucleic acid stabilization via electrostatic interactions.[5,6] Interactions between TDP-43 and cognate nucleic acid stabilizes splicesome complexes and facilitates mRNA maturation and nucleo-cytoplasmic transport.[7] Under normal conditions, TDP-43 is predominantly nuclear localized via an N-terminal nuclear localization sequence (NLS).[7–9] TDP-43 contains an intrinsically disordered C-terminal prion-like domain that harbors most familial mutations that are causative for amyotrophic lateral sclerosis (ALS) and frontotemporal lobar degeneration (FTLD).[10] Nevertheless, most sporadic ALS (sALS) cases lacking familial *TARDBP* mutations (~97% of cases) also exhibit TDP-43 pathology.[11,12]

Analyses of postmortem ALS tissue revealed that pathological TDP-43 contains many post-translational modifications (PTMs) including phosphorylation, ubiquitination, proteolytic cleavage, and more recently lysine acetylation.[13–17] Recent studies suggest that distinct PTMs may influence TDP-43 aggregate ultrastructure that correlates with clinical phenotypes in ALS and FTLD.[18–20] Our group previously assessed TDP-43 acetylation profiles in postmortem sALS tissue and discovered two putative acetylation sites (K145 and K192) that were less detectable in FTLD-TDP due to C-terminal TDP-43 cleavage.[17] In follow-up experiments, we introduced acetyl-mimic mutations at both sites (K145Q and K192Q) and found that the altered electrostatic properties disrupted interactions between TDP-43 and cognate nucleic acid, resulting in TDP-43 aggregation. A two-hit approach combining the acetyl-mimic mutations and NLS ablation (a combination mutant referred to as TDP-43-ΔNLS-KQ) caused cytoplasmic accumulation of phospho-409/410-positive TDP-43 aggregates that were strikingly similar to those observed in sALS.[21]

Given its aggregation propensity, we suspected that the two-hit TDP-43 variant may provide an ideal platform for the isolation of TDP-43 aggregates to evaluate their downstream pathogenic properties.

[1]Department of Cell Biology and Physiology, University of North Carolina at Chapel Hill, Chapel Hill, NC, USA

[2]Medical Student Training in Aging Research, Center for Aging and Health, University of North Carolina at Chapel Hill, Chapel Hill, NC, USA

[3]Proteomics Core Facility, Department of Pharmacology, University of North Carolina at Chapel Hill, Chapel Hill, NC, USA

[4]Department of Neurology, University of North Carolina at Chapel Hill, Chapel Hill, NC, USA

[5]Microscopy Services Laboratory, Department of Pathology and Laboratory Medicine, University of North Carolina at Chapel Hill, Chapel Hill, NC, USA

[6]Department of Biochemistry and Biophysics, University of North Carolina at Chapel Hill, Chapel Hill, NC, USA

[7]UNC Neuroscience Center, University of North Carolina at Chapel Hill, Chapel Hill, NC, USA

[8]Lead contact

*Correspondence: toddcohen@neurology.unc.edu

https://doi.org/10.1016/j.isci.2023.106645

This is an open access article under the CC BY-NC-ND license (http://creativecommons.org/licenses/by-nc-nd/4.0/).

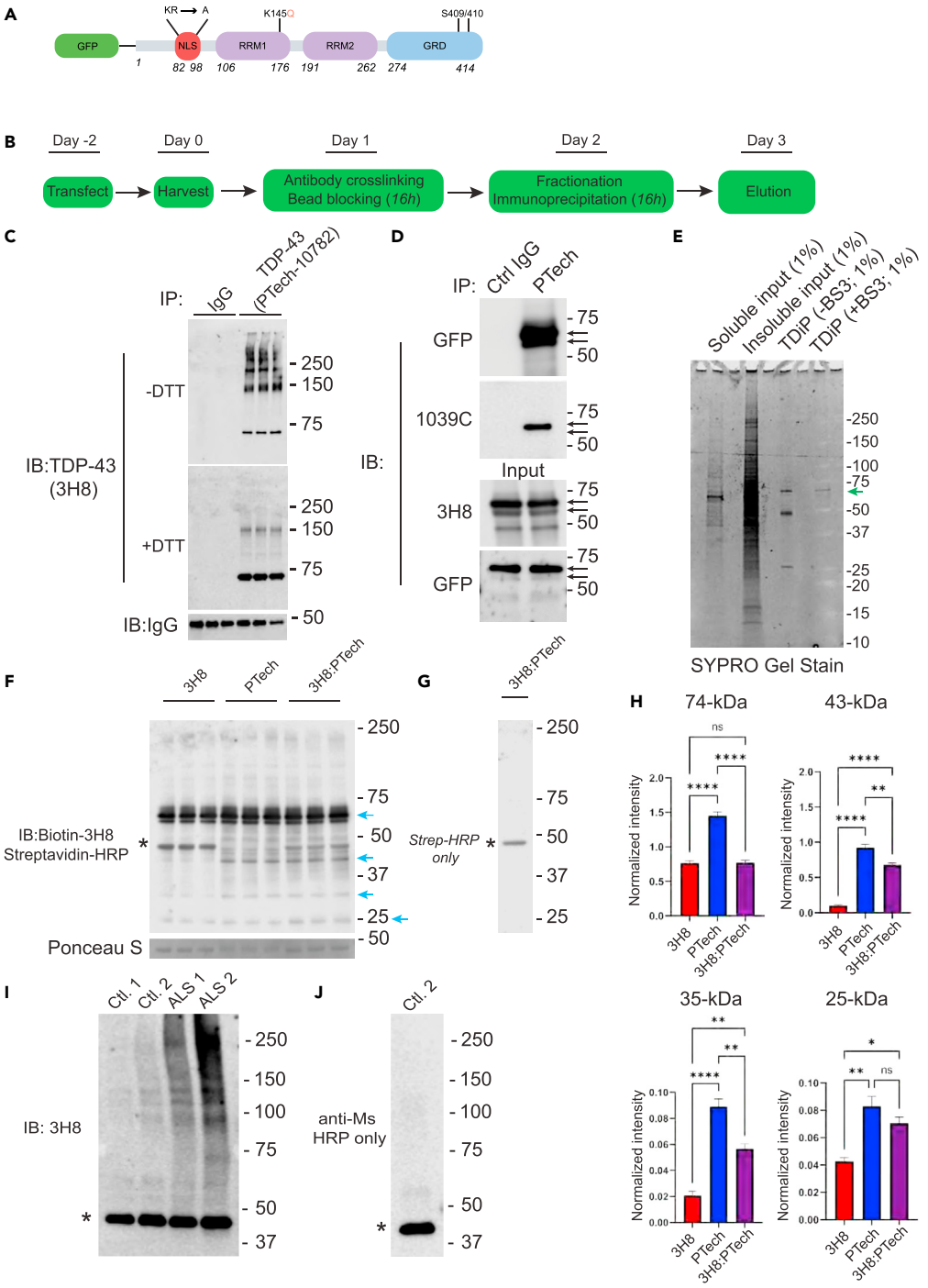

Figure 1. TDiP methodology allows for enrichment of pathological TDP-43 aggregates

(A) The TDP-43 construct (TDP-43-ΔNLS-KQ) contains an N-terminal GFP tag, mutated nuclear localization residues, K82A/R83A/K84A/K95A/K97A/R98A, and an acetyl-mimic mutation (K145Q) in the RRM1 domain. The molecular weight of the full-length TDP-43 fusion protein is ~74 kDa.

(B) Workflow for TDiP methodology.

(C) Reducing and non-reducing SDS-PAGE analysis of TDiP products shows that isolated TDP-43 aggregates are stabilized by disulfide linkages.

(D) Reducing SDS-PAGE of TDiP product shows prominent laddering bands around 74 kDa (TDP-43-GFP fusion protein) that are immunoreactive for GFP and pan-TDP-43 (3H8) but only a prominent 74 kDa band immunoreactive for C-terminal-specific 1039C (arrows), supporting the co-purification of TDP-43 fragments.

CellPress
OPEN ACCESS

Figure 1. *Continued*

(E) SYPRO Ruby total protein stain of soluble fraction, insoluble fraction, and eluted TDiP products, with and without BS3 antibody cross-linking, illustrating that TDP-43 can be purified without co-eluting IgG (derived from 10782-2-AP).

(F) High-sensitivity streptavidin-HRP blotting of TDiP samples using beads coupled to 15 μg monoclonal antibody 3H8, 15 μg polyclonal antibody 10782-2-AP, or 7.5 μg of each of 3H8 and 10782-2-AP shows increased yield of GFP-TDP-43 fusion protein (~70–74 kDa), endogenous (43 kDa) TDP-43 species, and pathological (25,-35 kDa) species when 10782-2-AP alone is used (turquoise arrows). Blots were blocked in non-protein-based blocking buffer, probed with biotinylated anti-TDP-43 (3H8), and imaged using Pierce High Sensitivity Streptavidin-HRP and enhanced chemiluminescence.

(G) The streptavidin-only blot to (F) showed non-specific cross-reactivity to a ~50 kDa biotinylated substrate (see asterisk at 50 kDa band).

(H) Quantification of (F); data are represented as mean ± SD, N = 3, p value one-way ANOVA (*$p < 0.05$, **$p<0.01$, ****$p<0.0001$).

(I) Non-reducing SDS-PAGE and immunoblot of TDiP preparations from the motor cortex of two non-neurological disease controls and sporadic ALS patients with confirmed TDP-43 pathology, highlighted by the ~50–250 kDa cross-linked TDP-43 multimers in ALS brain. Bead-bound cross-reactive IgG is shown as an internal loading control (asterisk).

(J) Secondary antibody-only control blot of 3H8 fidelity for detection of TDP-43 in tissue TDiP preparations. The asterisk denotes secondary antibody cross-reactivity when purifying TDP-43 using 10782-2-AP, as this antibody was not bead cross-linked to provide a loading reference.

This could overcome many of the limitations that have hampered TDP-43 model development. For example, it has been challenging to recreate TDP-43 pathology *in vitro*, as neither full-length wild-type nor familial ALS/FTLD mutant TDP-43 form robust aggregates in cell or neuronal models.[22–24] Other studies have turned to recombinant purified TDP-43 aggregates. While readily produced, critical TDP-43 PTMs are absent in *E. coli*-derived recombinant protein.[25] Although *in vitro* enzymatic modification protocols exist,[16] variation in the kinetics, fidelity, and efficiency introduces variability and may fail to recapitulate features derived *in situ*. Finally, as immunological studies begin to permeate the field of neurodegeneration,[26–29] caution must be taken when introducing *E. coli*-derived proteins to immune cells as trace amounts of endotoxins, such as lipopolysaccharide, can significantly confound immune phenotypes.[30]

Recently, several groups have published methods to enrich *in vivo* protein aggregates from postmortem tissue using detergent extraction and differential centrifugation.[19,31] However, the utility of the brain-extracted material is limited by (1) tissue accessibility and availability, (2) donor variability, (3) scalability, and (4) contaminating non-protein macromolecules that restrict downstream assay compatibility. Additionally, as more data become available to suggest there are disease subtype differences in TDP-43 pathology,[32] there may be an experimental need for both ALS- and FTLD-specific TDP-43 aggregates.

Here, we sought to develop a new approach to isolate pathological TDP-43 aggregates for downstream biochemical, proteomics, and cell-based assays. Using our previously established ALS-associated acetyl-mimic TDP-43 mutants, we developed **T**andem **D**etergent-extraction and **i**mmunoprecipitation of **P**roteinopathy (TDiP), a scalable immuno-purification method to generate human TDP-43 aggregates from a human cell culture model. This method preserves hallmark PTMs and maintains co-aggregating protein interactors with minimal contaminating debris. TDiP-isolated TDP-43 aggregates are customizable for *in vitro* assays including the use of modified fluorescent/epitope tags and amino acid substitutions. This approach may overcome prior limitations when studying the molecular underpinnings that drive TDP-43 pathogenesis.

RESULTS

TDiP immuno-purified TDP-43 aggregates from detergent-insoluble cell homogenates

While TDP-43 aggregates can be enriched using biochemical extractions, there is currently no method to reliably immuno-purify pathological TDP-43 from a scalable human model. Current centrifugation-based extraction approaches employ non-specific endonuclease (Benzonase) treatments to liberate core TDP-43 pathology from aggregated complexes. There is mounting evidence to suggest TDP-43 pathology formed *in situ* contains sequestered RNA and RNA-associated proteins.[33,34] Here, our goal was to preserve these interactions, so we selectively employed DNAse I for the degradation of genomic DNA.

We used our previously characterized GFP-tagged TDP-43-ΔNLS-KQ mutant to generate insoluble aggregates in Human Embryonic Kidney (HEK) HEK293A cells[21] (schematic, Figure 1A). We sought to preserve

TDP-43-RNA complexes within TDP-43 aggregates by combining a harsh detergent and DNase I treatment followed by immunoprecipitation (IP) to isolate pathological TDP-43 aggregates away from soluble factors, chromatin, and cellular debris (workflow, Figure 1B). Our IP procedure utilizes a commercially available and validated antibody (ProteinTech polyclonal 10782-2-AP) to pull down insoluble, disulfide cross-linked[35] TDP-43 aggregates (Figure 1C). We observed C-terminal TDP-43 cleavage, as demonstrated by a loss of C-terminal immunoreactivity (1039C) and preserved N-terminal GFP immunoreactivity (Figure 1D). We also noted lower molecular weight C-terminal fragments, namely 35- and 18-kDa, using 1039C (Figure S1). As an optional step dependent on downstream application, we optimized a modified antibody-bead cross-linking protocol[36] using Bissulfosuccinimidyl suberate (BS3) to remove the co-elution of immunoglobulin (IgG) heavy and light chains, and thereby maximize TDP-43 aggregate purity (Figure 1E).

We observed a significantly higher yield of TDP-43 aggregates using ProteinTech 10782-2-AP, compared to a validated monoclonal TDP-43 antibody (EMD Millipore 3H8). Furthermore, we found no evidence of increased yield when both antibodies were used in combination. Using ProteinTech 10782-2-AP, we noted a significantly higher yield of hallmark pathological C-terminal fragments, including ~25-kDa (Student's *t* test, $^{**}p < 0.01$), and 35-kDa (Student's *t* test, $^{****}p < 0.0001$)[14,37,38] relative to 3H8 (Figures 1F–1H). We also observed a significant increase in a band migrating at the molecular weight of endogenous human TDP-43 (Student's *t* test, $^{****}p < 0.0001$), suggesting that ectopically produced TDP-43 aggregates (i.e., TDP-43-ΔNLS-KQ) may be capable of recruiting endogenous TDP-43 in a templated manner that has been reported in ALS/FTLD.[3,20,32,39,40]

We provide a proof-of-concept validation that the TDiP method can be used to isolate disulfide-linked, phosphorylated TDP-43 aggregates that are present in low-abundance in the posterior frontal lobe (motor cortex) of postmortem ALS tissue. Using ~100 mg of frozen motor cortex from control and ALS cases as starting material (Table S1), TDP-43 was first sequentially extracted and confirmed to be hyper-phosphorylated and enriched in the insoluble fractions of ALS cases, but not controls (Figure S2). Next, TDiP was performed on brain extracts and the isolated, insoluble TDP-43 pathology was detected by non-reducing immunoblotting as distinct multimeric TDP-43 species ranging from ~50 to 250 kDa (Figure 1I). We used a secondary-only blot to more confidently identify TDP-43 species and exclude HRP-secondary antibody cross-reactivity to 10782-2-AP used in the pull-down (Figure 1J, asterisk). Despite the regional variability in TDP-43 pathology commonly observed in frozen post-mortem tissue, our purification yield and detection sensitivity were suitable for analysis of TDP-43 pathology in ALS brain. We note that further optimization may be required to conserve precious or rare CNS tissues including, for example, ALS spinal cord. The human tissue analysis substantiates the utility of the TDiP protocol and validates that our immuno-enrichment strategy (using anti-TDP-43, ProteinTech 10782-2-AP) is optimal for the isolation of disease-relevant TDP-43 species from both *in vitro* and *in vivo* sources.

We emphasize that the use of 10782-2-AP does not restrict enrichment to only the pathological C-terminal truncations or phosphorylated products, as might be the case with C-terminal (1039C) or phosphor-409/410 antibodies. Instead, we sought to develop a purification scheme that does not bias the purification toward specific pathological species but rather enriches those species as they occur *in situ*. For example, N-terminal TDP-43 fragments may also represent pathological TDP-43 signatures.[41–43] Therefore, the choice of TDP-43 antibody employed in the purification scheme can be tailored based on the user end goal (see STAR Methods).

TDiP-isolated TDP-43 complexes are protease resistant multimers

The limiting protease resistance assay is a common method to assess the conformation of protein aggregates identified across numerous neurodegenerative diseases.[18,19,44–51] To further characterize TDiP as a method of isolating ALS-associated TDP-43, we performed on-bead limiting proteinase-K (PK) digestion of TDP-43-ΔNLS-KQ aggregates, followed by non-reducing sodium dodecyl sulfate polyacrylamide gel electrophoresis (SDS-PAGE) analysis. As a reference for PK-*sensitive* TDP-43, we included soluble TDP-43-ΔNLS-KQ isolated by the same TDiP protocol and performed enzymatic treatment in parallel with the insoluble matieral. After treating the fractions with PK concentrations ranging from 0.04–2.5 μg/mL, we observed an overall increase in PK-resistance for the insoluble ~74, ~150, and ~250 kDa products when compared to their respective soluble counterparts (Figure 2A). Additionally, we observed that insoluble TDP-43 multimeric assemblies were more PK-resistant than insoluble TDP-43 monomer. Overall, we observed statistically significant differences in PK-resistance by two-way ANOVA with Bonferroni

CellPress
OPEN ACCESS

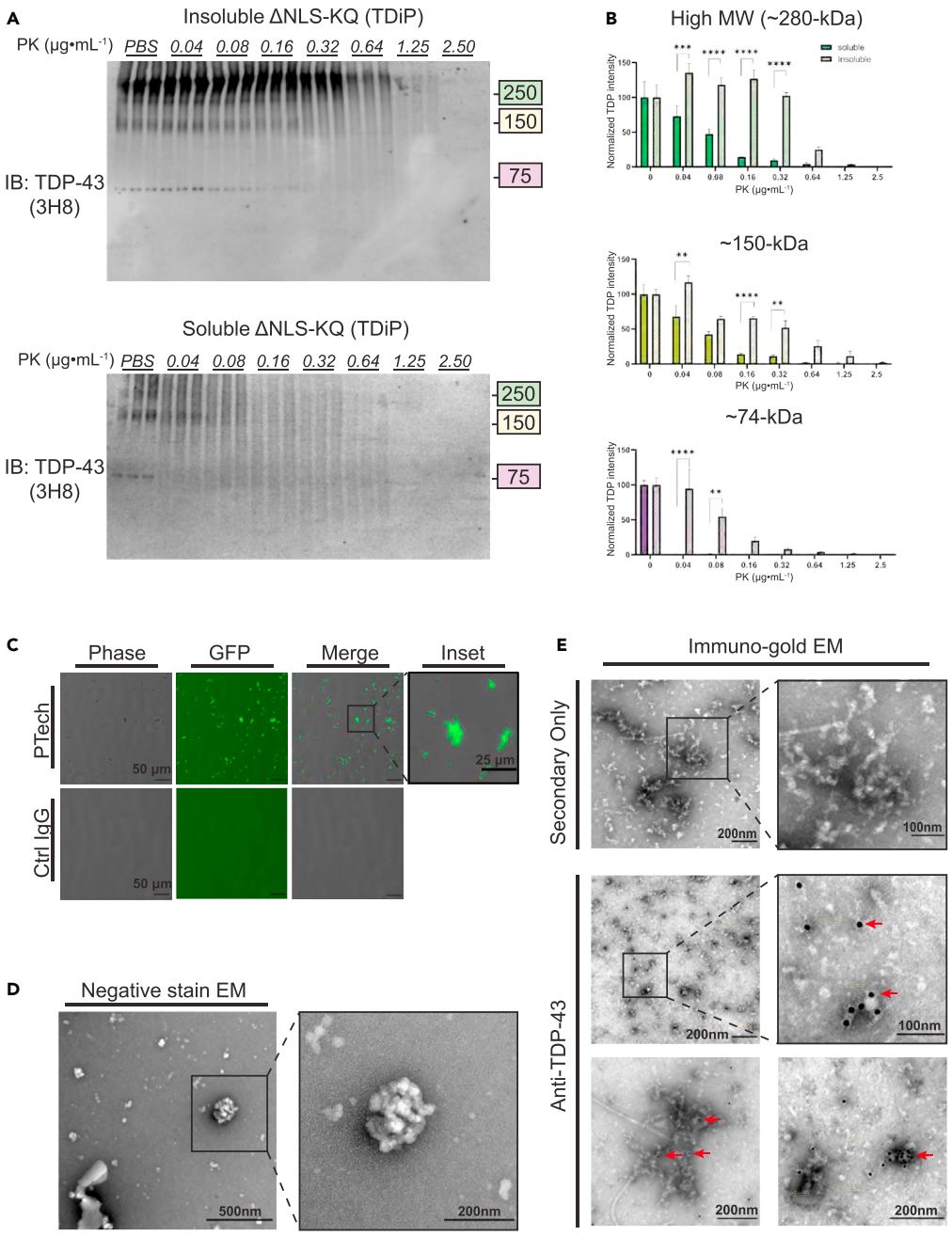

Figure 2. TDiP aggregates recapitulate the biochemical and structural signatures of ALS/FTLD brain extracts

(A) Limiting protease sensitivity assay of insoluble (top) and soluble (bottom) TDP-43-ΔNLS-KQ obtained by TDiP workflow. Non-reducing SDS-PAGE analysis reveals insoluble TDP-43 is more resistant to proteinase K (PK) digestion as compared to soluble TDP-43.

(B) Quantifications are based on the ~74 kDa full-length TDP-43 fusion protein band, as well as dimeric (~150 kDa) and tetrameric (~280-kDa) bands. Data are represented as mean ± SD, N ≥ 3, p value two-way ANOVA with Bonferroni correction (*$p < 0.05$, **$p < 0.01$, ***$p < 0.001$, ****$p < 0.0001$).

(C) Phase-contrast and epifluorescence micrographs of TDiP aggregate eluates (not sonicated) compared to eluates from control IgG antibody preparations. Elution with 5M NaCl preserves intrinsic GFP fluorescence with little observable debris.

(D) Ultrastructural characterization of TDiP aggregates (sonicated) by uranyl acetate negative staining transmission electron microscopy (TEM) reveals globular and largely disordered structures similar to those previously described using ALS/FTLD brain extracts.

(E) Immuno-gold electron microscopy validation of TDiP aggregates confirming their TDP-43 immunoreactivity.

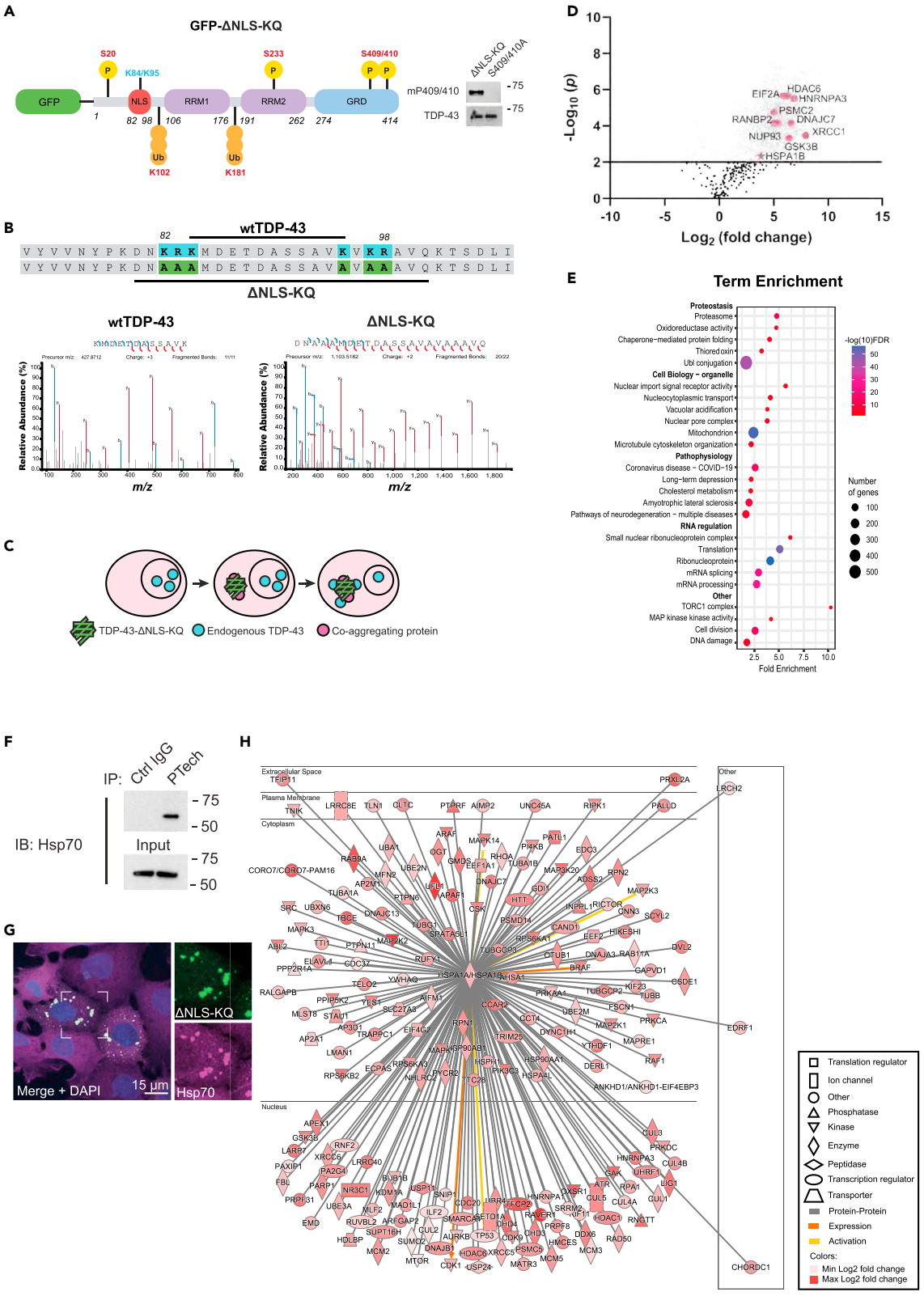
A
GFP-ΔNLS-KQ
S20
K84/K95
S233
S409/410
GFP
NLS
RRM1
RRM2
GRD
K102
K181
ΔNLS-KQ
S409/410A
mP409/410
TDP-43
B
wtTDP-43
ΔNLS-KQ
Relative Abundance (%)
m/z
C
TDP-43-ΔNLS-KQ
Endogenous TDP-43
Co-aggregating protein
D
-Log10 (p)
Log2 (fold change)
EIF2A
HDAC6
HNRNPA3
PSMC2
RANBP2
DNAJC7
XRCC1
NUP93
GSK3B
HSPA1B
E
Term Enrichment
Proteostasis
Proteasome
Oxidoreductase activity
Chaperone-mediated protein folding
Thioredoxin
Ubl conjugation
Cell Biology – organelle
Nuclear import signal receptor activity
Nucleocytoplasmic transport
Vacuolar acidification
Nuclear pore complex
Mitochondrion
Microtubule cytoskeleton organization
Pathophysiology
Coronavirus disease – COVID-19
Long-term depression
Cholesterol metabolism
Amyotrophic lateral sclerosis
Pathways of neurodegeneration – multiple diseases
RNA regulation
Small nuclear ribonucleoprotein complex
Translation
Ribonucleoprotein
mRNA splicing
mRNA processing
Other
TORC1 complex
MAP kinase kinase activity
Cell division
DNA damage
-log(10)FDR
Number of genes
Fold Enrichment
F
IP: Ctrl IgG PTech
IB: Hsp70
Input
G
Merge + DAPI
15 μm
ΔNLS-KQ
Hsp70
H
Extracellular Space
Plasma Membrane
Cytoplasm
Nucleus
Other
Translation regulator
Ion channel
Other
Phosphatase
Kinase
Enzyme
Peptidase
Transcription regulator
Transporter
Protein-Protein
Expression
Activation
Colors:
Min Log2 fold change
Max Log2 fold change

CellPress
OPEN ACCESS

Figure 3. TDiP aggregate proteome reveals disease-associated TDP-43 post-translational modifications (PTMs) and interactome

(A) Schematic depicting aggregated TDP-43 PTMs identified by mass spectrometry: phosphoserine (pS20), phospho-threonine (pT233), and ubiquitinated lysines (UbK102 and UbK181). Immunoblot validation of TDiP aggregate phosphorylation at disease-associated serine residues 409 and 410 (pS409/410). As a negative control, TDiP aggregates lacking S409/410 (TDP-43-ΔNLS-KQ-S409/410A) were used to abolish pS409/410 immunoreactivity.

(B) The tryptic peptide containing the TDP-43 residues mapping to the wild type TARDBP sequence with lysine (K84) and arginine (K95) was identified, suggesting TDiP aggregates composed of TDP-43-ΔNLS-KQ have seeding potential and can recruit endogenous wild-type TDP-43.

(C) Model of templated recruitment observed between TDP-43-ΔNLS-KQ and endogenous TDP-43.

(D) Volcano plot depicting protein interactors identified from N = 3 independent TDiP preparations. A 1% false discovery rate (FDR) was used to filter proteins and peptides. A $\log_2$ fold change (TDP vs. Isotype) was calculated using the normalized quantitative values and a $\log_2$ ratio ± 1 was considered significant.

(E) GO term and KEGG pathways enrichment analysis generated from, interacting proteins, sub-clustered by cellular process.

(F) Immunoblot validation of HSPA1B co-immunoprecipitation in TDiP isolates.

(G) Confocal micrograph of *in situ* TDP-43-ΔNLS-KQ aggregate co-localization with Hsp70 prior to TDiP purification. Scale bar, 15 μm.

(H) IPA network of HSPA1B and associated interactors stratified by sub-cellular distribution, protein class, and abundance.

correction in the following conditions: ~74-kDa (0.04 μg/mL, ****$p < 0.0001$ and 0.08 μg/mL, **$p = 0.0095$); ~150-kDa (0.04 μg/mL, ****$p = 0.0001$, 0.16 μg/mL, ****$p < 0.0001$, and 0.32 μg/mL, **$p = 0.0018$) and ~250-kDa (0.04 μg/mL, ***$p = 0.0006$, 0.08 μg/mL, ****$p < 0.0001$, 0.16 μg/mL, ****$p < 0.0001$, and 0.32 μg/mL, ****$p < 0.0001$) (Figure 2B). These *in vitro* data using TDP-43-ΔNLS-KQ generated aggregates are consistent with the biochemical signatures observed from brain-derived preparations.[18–20]

TDiP complexes recapitulate ultrastructural features identified *in vivo*

Our biochemical data thus far suggest the TDiP aggregates are largely insoluble, disulfide-linked, PK-resistant multimers. Therefore, we investigated the ultrastructural properties of the eluted products by phase-contrast/fluorescence microscopy and transmission electron microscopy (TEM). First, GFP-tagged TDP-43 aggregates were eluted from the TDiP matrix using 5M sodium chloride. We found this elution method best preserved intrinsic GFP autofluorescence allowing us to confirm aggregate fluorescence when overlayed with phase-contrast micrographs. We noted large, amorphous aggregates that were GFP-positive. By employing a negative control isolation in which TDP-43 aggregates were not enriched (IgG isotype control), we confirmed the absence of any contaminating cellular debris (Figure 2C). Next, we performed negative stain TEM and immunogold electron microscopy to further illustrate the ultrastructure of the eluted TDP-43 aggregates (Figures 2D and 2E). Qualitatively, these aggregates appeared as amorphous, globular species with rare fibrillar or classic amyloid-type structures, and resembled those isolated from brain extracts.[20,32,52]

The TDiP-isolated proteome reveals disease-associated interactors and post-translational modifications

Isolation of TDP-43 pathology from ALS-FTLD tissues is commonly associated with aberrant TDP-43 PTMs, C- and N-terminal truncations, and a broad interactome consisting of stress response proteins, and RNA-associated factors.[53,54] Here, we analyzed TDiP-isolated complexes by liquid chromatography-tandem mass spectrometry (LC-MS/MS)-based proteomics to identify TDP-43 disease-associated PTMs and any aggregate-associated protein interactions. As expected, TDP-43 peptides were abundant (log2 fold change = 5.10, $p < 1.7e^{-6.0}$, Student's *t* test) relative to profiles obtained from isotype controls (Table S2).

Disease-associated TDP-43 PTMs have been well characterized, most notably phosphorylation at serines 403/404 and 409/410 (pS409/410), ubiquitination, and truncation (TDP-35 and TDP-25 fragments). We performed PTM-mapping of TDiP-isolated TDP-43 to determine whether *in vivo* documented PTMs were present in our *in vitro* preparations (Figure 3A). We identified two phosphorylation sites at serine 20 and threonine 233. Although we initially did not identify hallmark phosphorylation sites pS409/410 by mass spectrometry due to lack of peptide coverage of the last 14-residues from the C-terminus, we nonetheless performed immunoblotting on TDiP-isolated TDP-43-ΔNLS-KQ versus a comparable phosphorylation-null aggregate variant (TDP-43-ΔNLS-KQ-S409/410A) to demonstrate antibody epitope specificity. Indeed, we detected robust pS409/410 in TDP-43-ΔNLS-KQ but not in TDP-43-ΔNLS-KQ-S409/410A TDiP products (Figure 3A). Additionally, we identified ubiquitination at K102 and K181.[37,54] Finally, we note the presence of an intact wild-type NLS containing K84 and K95 residues. Since these residues were mutated (K84A, K95A) in our ectopically expressed TDP-43-ΔNLS-KQ construct, it is likely these NLS intact peptides were detected due to recruitment and seeding of endogenous wild-type TDP-43 into the pathological aggregates (Figures 3B and 3C).

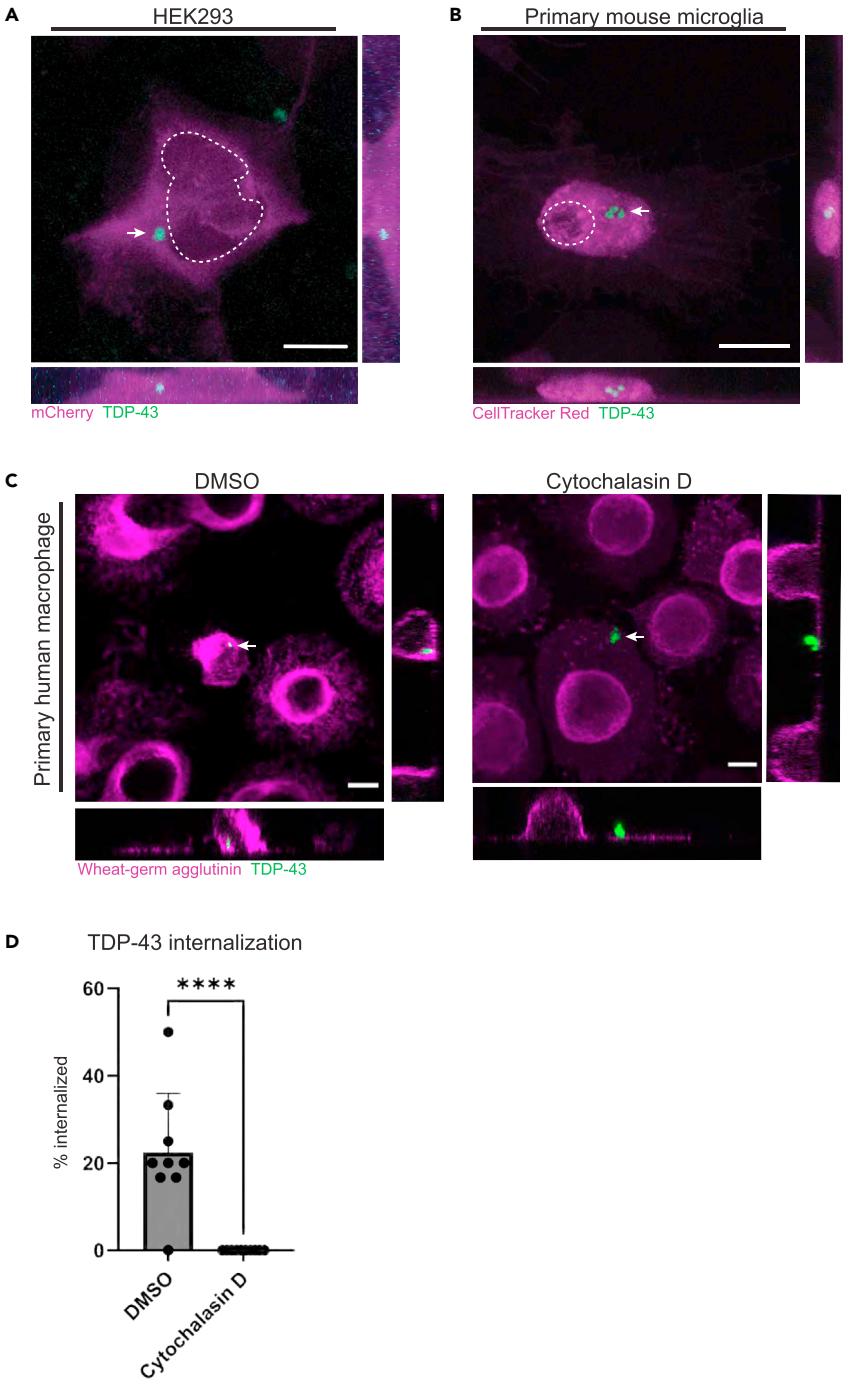

Figure 4. TDiP aggregates offer utility in cell-based internalization and trafficking assays

(A) Live-cell imaging of HEK293 cells that were whole-cell labeled with a control mCherry construct and transduced with TDiP aggregates using protein delivery reagent.

(B) Live-cell imaging of primary murine microglia with internalized TDiP aggregates. Microglia were labeled with CellTracker Red CMTPX dye and treated with aggregates (carrier-free).

(C) Live-cell imaging of primary human blood-derived macrophages following a 30-min incubation with TDiP aggregates (carrier-free) in the presence or absence of the phagocytosis inhibitor, Cytochalasin D. Scale bars, 10 μm. Dashed line, nuclei. Arrow, TDiP aggregate.

CellPress
OPEN ACCESS

Figure 4. *Continued*

(D) Quantification of internalization. Each data point represents the frequency of macrophages with internalized aggregates in a single randomized field of view. Data points depict all fields of view imaged across N = 2 independent experiments derived from two genetically different human donors. Data are represented as mean ± SD. Student's *t* test(****p = 0.0001).

We next characterized TDP-43 co-aggregating proteins. We identified several proteins involved in RNA regulation and nuclear maintenance (e.g., RANBP2 and Nup98), acute stress response pathways (e.g., EIF2a), and protein homeostasis (e.g., HSPA1B, DNAJC7, and PSMC2) (Figure 3D). Additionally, we identified other neurodegenerative disease associated-proteins, including Huntingtin,[55,56] VPS35 retromer complex component,[57] and neurofilament light chain (NEFL)[58,59] (Figure S3). Using Gene Ontology (GO) Term Enrichment and Kyoto Encyclopedia of Genes and Genomes (KEGG) analysis, we stratified protein interactors identified in the TDP-43 aggregates based on their cellular functions (Figure 3E).

We chose a known ALS- and TDP-43-associated molecular chaperone, HSPA1B encoding for Hsp70, for validation by immunoblot and confirmed its co-aggregation (Figure 3F). We then validated Hsp70 co-aggregation by confocal microscopy, in which TDP-43-ΔNLS-KQ cytoplasmic aggregates showed robust recruitment of Hsp70 (Figure 3G). This is in line with previous studies in which Hsp70 co-localized with TDP-43 pathology in postmortem tissue and cell models of disease.[21,60,61] To further support this interaction, we assessed the representation of other proteins in the HSPA1B pathway that were also sequestered in the TDP-43 aggregates using Ingenuity Pathway Analysis (IPA). Here, proteins were stratified by (1) sub-cellular localization, (2) protein class, and (3) fold enrichment of identified targets (Figure 3H). In total, 194 HSPA1B-interacting proteins were identified within TDP-43 aggregates across all major sub-cellular locations and functional classes. Their recruitment suggests TDP-43-mediated perturbation of the HSPA1B signaling, which may contribute to cellular dysfunction associated with TDP-43 pathology.

TDiP-isolated TDP-43 aggregate are internalized in a cell-type dependent manner

A central question in TDP-43 pathogenesis is the ability of protein aggregates to propagate throughout the brain parenchyma in a prion-like manner. Multiple theories of protein aggregate transmission exist, including direct neuronal uptake via micropinocytosis and indirect transfer via professional phagocytes harboring protein aggregates (e.g., brain-resident macrophages and microglia).[62–65] To determine whether TDiP-isolated aggregates have utility in TDP-43 internalization assays, we examined aggregate uptake using multiple cell culture models (Figure 4).

First, we assessed TDP-43 aggregate uptake in non-phagocytic HEK 293 cells, as previously shown with brain-derived TDP-43 aggregates.[19,20,40] Indeed, we confirmed TDP-43 aggregate transduction using a protein delivery agent, and uptake by confocal microscopy (Figure 4A, arrows). We next sought to explore aggregate phagocytosis and uptake using *bona fide* phagocytic cells, including primary mouse microglia and human macrophages, which have been implicated in aggregate trafficking and spreading in disease pathogenesis.[65,66] We took advantage of the intrinsic fluorescent properties of our GFP-labeled TDiP product to directly monitor internalization. We first qualitatively used live-cell imaging and observed uptake in primary mouse microglia using a cell-fill protein stain to observe intracellular protein displacement caused by the aggregate (Figure 4B). Next, we quantitatively interrogated the mechanism of internalization in primary human macrophages. Here, we observed robust uptake of TDiP aggregates in macrophages as demonstrated by the containment of a GFP-positive TDiP aggregate within the macrophage plasma membrane previously labeled with fluorescent wheat-germ agglutinin (WGA-647). Moreover, this phenotype was ablated upon treatment with cytochalasin D, a standard pharmacological inhibitor of actin-mediated phagocytosis and micropinocytosis[67–70] (Figures 4C and 4D). Thus, our TDiP-derived aggregates also offer utility in live cell-based assays capable of monitoring aggregate internalization and trafficking, including innate immune cells that are particularly sensitive to endotoxins and other non-protein contaminants.

DISCUSSION

Here, we describe TDiP as a streamlined and scalable method to produce TDP-43 pathology from cells and tissues. It has been challenging to develop models of mature TDP-43 aggregation relevant to ALS/FTD, as many commonly used familial TDP-43 mutants do not form robust intracellular aggregates in cellular model systems. Furthermore, while the expression of C-terminal TDP-43 fragments can accelerate TDP-43 aggregate formation in eukaryotic and prokaryotic cell models, their use is limited when studying the properties

Table 1. Schematic depicting the advantages of the TDiP method in the context of other established methods for purification and analysis of pathological TDP-43

	TDiP	Tissue Extraction	Recombinant
Scalable	++	+	+++
Affinity purified	+	-	−/+
Endotoxin free	+	+	−/+
Modifiable protein sequence (e.g., epitope tags)	+	-	+
Accessible source of aggregates	+	−/+	+++
In situ TDP-43 aggregation	+	+	-
Presence of TDP-43 post-translational modifications (PTMs)	+	+	-

of full-length TDP-43. Thus, we reasoned that by driving TDP-43 to the cytoplasm and simultaneously destabilizing the TDP-43:RNA interaction via the K145Q substitution that we previously discovered,[17] we could theoretically purify ample amounts of pathological TDP-43 that are suitable for many downstream applications including, for example, assessment of TDP-43 aggregate-release mechanisms, cellular uptake, and prion-like spreading.

Our immuno-enrichment method of purifying TDP-43-ΔNLS-KQ aggregates retained many of the hallmark characteristics of ALS pathology including detergent insolubility, disulfide cross-linked TDP-43 multimers,[15,35,43,71] and TDP-43 truncations.[14,38,53] We validated these biochemical characteristics by using a limiting protease resistance assay to demonstrate their resistance to proteolytic cleavage at increasing PK concentrations when compared to soluble TDP-43-ΔNLS-KQ, which is consistent with brain-extracted material.[18,19,31] Moreover, we observed that the amorphous and structurally disorganized nature of TDP-43-ΔNLS-KQ aggregates by immunogold TEM is consistent with other published TDP-43 aggregates.[18–20,72–74]

We further expanded on the utility of this method using a systems-based proteomics approach to identify co-aggregating factors that may drive TDP-43 pathogenesis. Our analysis revealed ~2000 TDP-43-associated proteins present in the TDP-43 aggregate preparation, but not the isotype controls. Some of these hits have been validated as TDP-43 interactors including HSPA1,[21] HTT,[56] and 26S proteasome regulatory subunit 4 (PSMC2).[72] Interestingly, we identified a broad subset of functional categories and signaling pathways that interact with TDiP purified aggregates, notably other ALS-relevant proteins (e.g., MATRN-3 and TBK-1), apoptotic regulators (e.g., APAF-1 and p53), a large subset of proteasome subunits, chaperones (e.g., DNAJ family members, Hsp70, and Hsp90), and general proteostasis regulators (e.g., HDAC6). Their co-aggregation with TDP-43 is consistent with the active processing and/or triaging of aggregated TDP-43 as a cellular defense mechanism and activation of a protein quality control response.

TDP-43 is thought to spread in a prion-like manner by a release/uptake mechanism through neuroanatomical networks or surrounding cells such as glia for disease propagation.[14,29,55,66] Indeed, delivery of FTLD-TDP brain extracts using *in vitro* and *in vivo* models is sufficient to induce templated seeding and spread of TDP-43 pathology in recipient cells.[18–20,32,40,55,74] However, dependence on ALS spinal cord tissue can be problematic due to prominent motor neuron loss (i.e., minimal yields of extracted TDP-43 pathology) and inherent limitations concerning tissue sample availability/accessibility. Therefore, we reasoned that TDiP-isolated aggregates from scalable HEK293 cultures could be used to evaluate internalization in different cell types. We confirmed that TDiP aggregates were transduced into non-phagocytic HEK293 cells with a protein delivery agent. Recent studies also suggest that TDP-43 aggregate uptake is not simply limited to neurons as both microglia and astrocytes can internalize pathological TDP-43.[14,29,55,66] Indeed, we observed carrier-free TDiP aggregate phagocytosis by primary human macrophages and mouse microglia using live-cell imaging, which was impaired by cytochalasin D treatment. To our knowledge, this is the first demonstration that *in situ*-derived, traceable TDP-43 aggregates are amenable to internalization assays using glia and analogous peripheral immune cells. Thus, our methodology could encourage the development of more robust, precise, and sensitive assays to interrogate TDP-43 uptake, spread, and propagation.

Taken together, the development of TDiP provides an additional modality to enrich TDP-43 pathology that is suitable for downstream characterization and cell-based assays (Table 1). Since TDiP-derived aggregates

CellPress
OPEN ACCESS

display many of the biochemical properties of TDP-43 pathology isolated from ALS/FTLD brain and spinal cord, this could overcome many limitations in studying the properties of disease-associated TDP-43 aggregates. TDiP, therefore, opens up avenues for biochemical and cell-based investigation of TDP-43 pathophysiology as well as opportunities for drug development and drug screening to target and suppress TDP-43 aggregation.

Limitations of the study

Although HEK293 cells are regarded as neuron-like,[75] we cannot exclude the possibility that TDP-43 co-aggregating proteins differ in mitotic versus post-mitotic cell types such as neurons. Although cell-type specific comparisons of TDiP aggregate composition were not the primary goal of this study, and given mounting evidence of TDP-43 pathology in multiple diverse cell types (e.g., muscle, neurons, immune cells, glia), current efforts are underway to evaluate cell-type specific compositional differences of the TDP-43 aggregate interactome.

STAR★METHODS

Detailed methods are provided in the online version of this paper and include the following:

- KEY RESOURCES TABLE
- RESOURCE AVAILABILITY
  - Lead contact
  - Materials availability
  - Data and code availability
- EXPERIMENTAL MODEL AND SUBJECT DETAILS
- METHOD DETAILS
  - Plasmid construction
  - Cell culture and transfection
  - Primary macrophage culture
  - Tandem detergent-extraction and immunoprecipitation of proteinopathy (TDiP)
  - Immunoblotting
  - Limiting proteinase resistance assay
  - Negative stain and immunogold electron microscopy
  - Proteomics analysis
  - Immunofluorescence
  - Confocal microscopy
  - Live-cell HEK293 protein transduction assay
  - Live-cell microglia phagocytosis assay
  - Live-cell human macrophage phagocytosis assay
- QUANTIFICATION AND STATISTICAL ANALYSIS

SUPPLEMENTAL INFORMATION

Supplemental information can be found online at https://doi.org/10.1016/j.isci.2023.106645.

ACKNOWLEDGMENTS

We thank Dr. Giulia Fragola for additional review of the manuscript. This research is based in part upon work conducted using the UNC Proteomics Core Facility, which is supported in part by P30 CA016086 Cancer Center Core Support Grant to the UNC Lineberger Comprehensive Cancer Center. The Microscopy Services Laboratory, Department of Pathology and Laboratory Medicine, is supported in part by P30 CA016086 Cancer Center Core Support Grant to the UNC Lineberger Comprehensive Cancer Center. We thank Dr. Ian Robey and the Department of Veterans Affairs ALS Biorespository, merit review BX002466.

This work was supported in part by the United States National Institutes of Health (NIH) grants R01AG061188, R01NS105981, and R21AG058080 (T.J.C.); National Science Foundation DGE-1650116 and NIH F31NS122242 (B.A.E.); NIH T35AG038047 (S.R.C.); NIH R01 NS108808 (R.M.); NIH R35GM133460 (S.C.); NIH F30 AG 072786 and 1T32GM133364-01A1 (J.C.N). The content is the responsibility of the authors and does not necessarily represent the official views of the National Institutes of Health.

AUTHOR CONTRIBUTIONS

B.A.E. and T.J.C., conceptualization. B.A.E., S.R.C., T.A., L.H., A.H., N.B., R.J.P., J.C.N, K.W., R.M., J.V.R., and S.C., investigation. X.T., plasmid construction. B.A.E. and T.J.C., writing—original draft. All authors reviewed, edited, and approved the final version of this manuscript.

DECLARATION OF INTERESTS

The authors declare no conflicts of interest with the contents of this article.

INCLUSION AND DIVERSITY

One or more of the authors of this paper self-identifies as a member of the LGBTQIA+ community. We support inclusive, diverse, and equitable conduct of research.

Received: October 24, 2022
Revised: January 3, 2023
Accepted: April 5, 2023
Published: April 11, 2023

REFERENCES

1. Sephton, C.F., Cenik, C., Kucukural, A., Dammer, E.B., Cenik, B., Han, Y., Dewey, C.M., Roth, F.P., Herz, J., Peng, J., et al. (2011). Identification of neuronal RNA targets of TDP-43-containing ribonucleoprotein complexes. J. Biol. Chem. *286*, 1204–1215. https://doi.org/10.1074/JBC.M110.190884.

2. Tollervey, J.R., Curk, T., Rogelj, B., Briese, M., Cereda, M., Kayikci, M., König, J., Hortobágyi, T., Nishimura, A.L., Zupunski, V., et al. (2011). Characterizing the RNA targets and position-dependent splicing regulation by TDP-43. Nat. Neurosci. *14*, 452–458. https://doi.org/10.1038/NN.2778.

3. Ling, S.C., Polymenidou, M., and Cleveland, D.W. (2013). Converging mechanisms in ALS and FTD: disrupted RNA and protein homeostasis. Neuron *79*, 416–438. https://doi.org/10.1016/J.NEURON.2013.07.033.

4. Polymenidou, M., Lagier-Tourenne, C., Hutt, K.R., Huelga, S.C., Moran, J., Liang, T.Y., Ling, S.C., Sun, E., Wancewicz, E., Mazur, C., et al. (2011). Long pre-mRNA depletion and RNA missplicing contribute to neuronal vulnerability from loss of TDP-43. Nat. Neurosci. *14*, 459–468. https://doi.org/10.1038/NN.2779.

5. Kuo, P.H., Doudeva, L.G., Wang, Y.T., Shen, C.K.J., and Yuan, H.S. (2009). Structural insights into TDP-43 in nucleic-acid binding and domain interactions. Nucleic Acids Res. *37*, 1799–1808. https://doi.org/10.1093/NAR/GKP013.

6. Kuo, P.H., Chiang, C.H., Wang, Y.T., Doudeva, L.G., and Yuan, H.S. (2014). The crystal structure of TDP-43 RRM1-DNA complex reveals the specific recognition for UG- and TG-rich nucleic acids. Nucleic Acids Res. *42*, 4712–4722. https://doi.org/10.1093/NAR/GKT1407.

7. Winton, M.J., Igaz, L.M., Wong, M.M., Kwong, L.K., Trojanowski, J.Q., and Lee, V.M.Y. (2008). Disturbance of nuclear and cytoplasmic TAR DNA-binding protein (TDP-43) induces disease-like redistribution, sequestration, and aggregate formation. J. Biol. Chem. *283*, 13302–13309. https://doi.org/10.1074/JBC.M800342200.

8. Archbold, H.C., Jackson, K.L., Arora, A., Weskamp, K., Tank, E.M.H., Li, X., Miguez, R., Dayton, R.D., Tamir, S., Klein, R.L., and Barmada, S.J. (2018). TDP43 nuclear export and neurodegeneration in models of amyotrophic lateral sclerosis and frontotemporal dementia. Sci. Rep. *8*, 4606. https://doi.org/10.1038/S41598-018-22858-W.

9. Pinarbasi, E.S., Cağatay, T., Fung, H.Y.J., Li, Y.C., Chook, Y.M., and Thomas, P.J. (2018). Active nuclear import and passive nuclear export are the primary determinants of TDP-43 localization. Sci. Rep. *8*, 7083. https://doi.org/10.1038/S41598-018-25008-4.

10. Suk, T.R., and Rousseaux, M.W.C. (2020). The role of TDP-43 mislocalization in amyotrophic lateral sclerosis. Mol. Neurodegener. *15*, 45. https://doi.org/10.1186/S13024-020-00397-1.

11. Hardiman, O., Al-Chalabi, A., Chio, A., Corr, E.M., Logroscino, G., Robberecht, W., Shaw, P.J., Simmons, Z., and Van Den Berg, L.H. (2017). Amyotrophic lateral sclerosis. Nat. Rev. Dis. Primers *3*, 17071. https://doi.org/10.1038/NRDP.2017.71.

12. Mackenzie, I.R.A., Bigio, E.H., Ince, P.G., Geser, F., Neumann, M., Cairns, N.J., Kwong, L.K., Forman, M.S., Ravits, J., Stewart, H., et al. (2007). Pathological TDP-43 distinguishes sporadic amyotrophic lateral sclerosis from amyotrophic lateral sclerosis with SOD1 mutations. Ann. Neurol. *61*, 427–434. https://doi.org/10.1002/ANA.21147.

13. Kwong, L.K., Uryu, K., Trojanowski, J.Q., and Lee, V.M.Y. (2008). TDP-43 proteinopathies: neurodegenerative protein misfolding diseases without amyloidosis. Neurosignals. *16*, 41–51. https://doi.org/10.1159/000109758.

14. Zhang, Y.J., Xu, Y.F., Cook, C., Gendron, T.F., Roettges, P., Link, C.D., Lin, W.L., Tong, J., Castanedes-Casey, M., Ash, P., et al. (2009). Aberrant cleavage of TDP-43 enhances aggregation and cellular toxicity. Proc. Natl. Acad. Sci. USA *106*, 7607–7612. https://doi.org/10.1073/PNAS.0900688106.

15. Buratti, E. (2018). TDP-43 post-translational modifications in health and disease. Expert Opin. Ther. Targets *22*, 279–293. https://doi.org/10.1080/14728222.2018.1439923.

16. Hasegawa, M., Arai, T., Nonaka, T., Kametani, F., Yoshida, M., Hashizume, Y., Beach, T.G., Buratti, E., Baralle, F., Morita, M., et al. (2008). Phosphorylated TDP-43 in frontotemporal lobar degeneration and amyotrophic lateral sclerosis. Ann. Neurol. *64*, 60–70. https://doi.org/10.1002/ANA.21425.

17. Cohen, T.J., Hwang, A.W., Restrepo, C.R., Yuan, C.X., Trojanowski, J.Q., and Lee, V.M.Y. (2015). An acetylation switch controls TDP-43 function and aggregation propensity. Nat. Commun. *6*, 5845. https://doi.org/10.1038/ncomms6845.

18. Porta, S., Xu, Y., Lehr, T., Zhang, B., Meymand, E., Olufemi, M., Stieber, A., Lee, E.B., Trojanowski, J.Q., and Lee, V.M.Y. (2021). Distinct brain-derived TDP-43 strains from FTLD-TDP subtypes induce diverse morphological TDP-43 aggregates and spreading patterns in vitro and in vivo. Neuropathol. Appl. Neurobiol. *47*, 1033–1049. https://doi.org/10.1111/NAN.12732.

19. Porta, S., Xu, Y., Restrepo, C.R., Kwong, L.K., Zhang, B., Brown, H.J., Lee, E.B., Trojanowski, J.Q., and Lee, V.M.Y. (2018). Patient-derived frontotemporal lobar degeneration brain extracts induce formation and spreading of TDP-43 pathology in vivo. Nat. Commun. *9*, 4220. https://doi.org/10.1038/S41467-018-06548-9.

20. Laferrière, F., Maniecka, Z., Pérez-Berlanga, M., Hruska-Plochan, M., Gilhespy, L., Hock, E.M., Wagner, U., Afroz, T., Boersema, P.J., Barmettler, G., et al. (2019). TDP-43 extracted from frontotemporal lobar degeneration subject brains displays distinct aggregate assemblies and neurotoxic effects reflecting disease progression rates. Nat. Neurosci. *22*,

65–77. https://doi.org/10.1038/S41593-018-0294-Y.

21. Wang, P., Wander, C.M., Yuan, C.X., Bereman, M.S., and Cohen, T.J. (2017). Acetylation-induced TDP-43 pathology is suppressed by an HSF1-dependent chaperone program. Nat. Commun. *8*, 82. https://doi.org/10.1038/s41467-017-00088-4.

22. Arnold, E.S., Ling, S.C., Huelga, S.C., Lagier-Tourenne, C., Polymenidou, M., Ditsworth, D., Kordasiewicz, H.B., McAlonis-Downes, M., Platoshyn, O., Parone, P.A., et al. (2013). ALS-linked TDP-43 mutations produce aberrant RNA splicing and adult-onset motor neuron disease without aggregation or loss of nuclear TDP-43. Proc. Natl. Acad. Sci. USA *110*, E736–E745. https://doi.org/10.1073/PNAS.1222809110.

23. Pesiridis, G.S., Lee, V.M.Y., and Trojanowski, J.Q. (2009). Mutations in TDP-43 link glycine-rich domain functions to amyotrophic lateral sclerosis. Hum. Mol. Genet. *18*, R156–R162. https://doi.org/10.1093/HMG/DDP303.

24. Baloh, R.H. (2011). TDP-43: the relationship between protein aggregation and neurodegeneration in amyotrophic lateral sclerosis and frontotemporal lobar degeneration. FEBS J. *278*, 3539–3549. https://doi.org/10.1111/J.1742-4658.2011.08256.X.

25. Wingfield, P.T. (2015). Overview of the purification of recombinant proteins. Curr. Protoc. Protein Sci. *80*, 6.1.1–6.1.35. https://doi.org/10.1002/0471140864.PS0601S80.

26. McCauley, M.E., and Baloh, R.H. (2019). Inflammation in ALS/FTD pathogenesis. Acta Neuropathol. *137*, 715–730. https://doi.org/10.1007/S00401-018-1933-9.

27. Saba, J., Couselo, F.L., Bruno, J., Carniglia, L., Durand, D., Lasaga, M., and Caruso, C. (2022). Neuroinflammation in huntington's disease: a starring role for astrocyte and microglia. Curr. Neuropharmacol. *20*, 1116–1143. https://doi.org/10.2174/1570159X19666211201094608.

28. Rocha, E.M., De Miranda, B., and Sanders, L.H. (2018). Alpha-synuclein: pathology, mitochondrial dysfunction and neuroinflammation in Parkinson's disease. Neurobiol. Dis. *109*, 249–257. https://doi.org/10.1016/J.NBD.2017.04.004.

29. Heneka, M.T., Carson, M.J., El Khoury, J., Landreth, G.E., Brosseron, F., Feinstein, D.L., Jacobs, A.H., Wyss-Coray, T., Vitorica, J., Ransohoff, R.M., Herrup, K., et al. (2015). Neuroinflammation in Alzheimer's disease. Lancet Neurol. *14*, 388–405. https://doi.org/10.1016/S1474-4422(15)70016-5.

30. Batista, C.R.A., Gomes, G.F., Candelario-Jalil, E., Fiebich, B.L., and de Oliveira, A.C.P. (2019). Lipopolysaccharide-Induced neuroinflammation as a bridge to understand neurodegeneration. Int. J. Mol. Sci. *20*, 2293. https://doi.org/10.3390/IJMS20092293.

31. Manuela, P.-B., Florent, L., and Magdalini, P. (2019). SarkoSpin: a technique for biochemical isolation and characterization of pathological TDP-43 aggregates. Bio Protoc. *9*, e3424. https://doi.org/10.21769/BIOPROTOC.3424.

32. De Rossi, P., Lewis, A.J., Furrer, J., De Vos, L., Demeter, T., Zbinden, A., Zhong, W., Wiersma, V.I., Scialo, C., Weber, J., et al. (2021). FTLD-TDP assemblies seed neoaggregates with subtype-specific features via a prion-like cascade. EMBO Rep. *22*, e53877. https://doi.org/10.15252/EMBR.202153877.

33. Droppelmann, C.A., Campos-Melo, D., Moszczynski, A.J., Amzil, H., and Strong, M.J. (2019). TDP-43 aggregation inside micronuclei reveals a potential mechanism for protein inclusion formation in ALS. Sci. Rep. *91*, 19928. https://doi.org/10.1038/s41598-019-56483-y.

34. Zuo, X., Zhou, J., Li, Y., Wu, K., Chen, Z., Luo, Z., Zhang, X., Liang, Y., Esteban, M.A., Zhou, Y., and Fu, X.D. (2021). TDP-43 aggregation induced by oxidative stress causes global mitochondrial imbalance in ALS. Nat. Struct. Mol. Biol. *28*, 132–142. https://doi.org/10.1038/S41594-020-00537-7.

35. Cohen, T.J., Hwang, A.W., Unger, T., Trojanowski, J.Q., and Lee, V.M.Y. (2012). Redox signalling directly regulates TDP-43 via cysteine oxidation and disulphide cross-linking. EMBO J. *31*, 1241–1252. https://doi.org/10.1038/EMBOJ.2011.471.

36. Jiang, P., Gan, M., Yen, S.H., McLean, P.J., and Dickson, D.W. (2017). Impaired endo-lysosomal membrane integrity accelerates the seeding progression of α-synuclein aggregates. Sci. Rep. *7*, 7690. https://doi.org/10.1038/S41598-017-08149-W.

37. Neumann, M., Sampathu, D.M., Kwong, L.K., Truax, A.C., Micsenyi, M.C., Chou, T.T., Bruce, J., Schuck, T., Grossman, M., Clark, C.M., et al. (2006). Ubiquitinated TDP-43 in frontotemporal lobar degeneration and amyotrophic lateral sclerosis. Science *314*, 130–133. https://doi.org/10.1126/SCIENCE.1134108.

38. Berning, B.A., and Walker, A.K. (2019). The pathobiology of TDP-43 C-terminal fragments in ALS and FTLD. Front. Neurosci. *13*, 335. https://doi.org/10.3389/FNINS.2019.00335.

39. Polymenidou, M., and Cleveland, D.W. (2011). The seeds of neurodegeneration: prion-like spreading in ALS. Cell *147*, 498–508. https://doi.org/10.1016/J.CELL.2011.10.011.

40. Nonaka, T., Masuda-Suzukake, M., Arai, T., Hasegawa, Y., Akatsu, H., Obi, T., Yoshida, M., Murayama, S., Mann, D.M.A., Akiyama, H., and Hasegawa, M. (2013). Prion-like properties of pathological TDP-43 aggregates from diseased brains. Cell Rep. *4*, 124–134. https://doi.org/10.1016/J.CELREP.2013.06.007.

41. Romano, V., Quadri, Z., Baralle, F.E., and Buratti, E. (2015). The structural integrity of TDP-43 N-terminus is required for efficient aggregate entrapment and consequent loss of protein function. Prion *9*, 1–9. https://doi.org/10.1080/19336896.2015.1011885.

42. Chang, C.k., Wu, T.H., Wu, C.Y., Chiang, M.h., Toh, E.K.W., Hsu, Y.C., Lin, K.F., Liao, Y.h., Huang, T.H., and Huang, J.J.T. (2012). The N-terminus of TDP-43 promotes its oligomerization and enhances DNA binding affinity. Biochem. Biophys. Res. Commun. *425*, 219–224. https://doi.org/10.1016/J.BBRC.2012.07.071.

43. Jiang, L.L., Xue, W., Hong, J.Y., Zhang, J.T., Li, M.J., Yu, S.N., He, J.H., and Hu, H.Y. (2017). The N-terminal dimerization is required for TDP-43 splicing activity. Sci. Rep. *7*, 6196. https://doi.org/10.1038/s41598-017-06263-3.

44. Baiardi, S., Rossi, M., Mammana, A., Appleby, B.S., Barria, M.A., Calì, I., Gambetti, P., Gelpi, E., Giese, A., Ghetti, B., et al. (2021). Phenotypic diversity of genetic Creutzfeldt-Jakob disease: a histo-molecular-based classification. Acta Neuropathol. *142*, 707–728. https://doi.org/10.1007/S00401-021-02350-Y.

45. Aguzzi, A., Heikenwalder, M., and Polymenidou, M. (2007). Insights into prion strains and neurotoxicity. Nat. Rev. Mol. Cell Biol. *8*, 552–561. https://doi.org/10.1038/NRM2204.

46. Guo, J.L., Covell, D.J., Daniels, J.P., Iba, M., Stieber, A., Zhang, B., Riddle, D.M., Kwong, L.K., Xu, Y., Trojanowski, J.Q., and Lee, V.M.Y. (2013). Distinct α-synuclein strains differentially promote tau inclusions in neurons. Cell *154*, 103–117. https://doi.org/10.1016/J.CELL.2013.05.057.

47. Li, L., Shi, R., Gu, J., Tung, Y.C., Zhou, Y., Zhou, D., Wu, R., Chu, D., Jin, N., Deng, K., et al. (2021). Alzheimer's disease brain contains tau fractions with differential prion-like activities. Acta Neuropathol. Commun. *9*, 28. https://doi.org/10.1186/S40478-021-01127-4.

48. Shuster, S.O., and Lee, J.C. (2021). Tryptophan probes of TDP-43 C-terminal domain amyloid formation. J. Phys. Chem. B *125*, 3781–3789. https://doi.org/10.1021/ACS.JPCB.1C00767.

49. Kushnirov, V.V., Dergalev, A.A., and Alexandrov, A.I. (2020). Proteinase K resistant cores of prions and amyloids. Prion *14*, 11–19. https://doi.org/10.1080/19336896.2019.1704612.

50. Shahnawaz, M., Mukherjee, A., Pritzkow, S., Mendez, N., Rabadia, P., Liu, X., Hu, B., Schmeichel, A., Singer, W., Wu, G., et al. (2020). Discriminating α-synuclein strains in Parkinson's disease and multiple system atrophy. Nature *578*, 273–277. https://doi.org/10.1038/S41586-020-1984-7.

51. Tsuji, H., Arai, T., Kametani, F., Nonaka, T., Yamashita, M., Suzukake, M., Hosokawa, M., Yoshida, M., Hatsuta, H., Takao, M., et al. (2012). Molecular analysis and biochemical classification of TDP-43 proteinopathy. Brain. *135*, 3380–3391. https://doi.org/10.1093/BRAIN/AWS230.

52. Afroz, T., Hock, E.M., Ernst, P., Foglieni, C., Jambeau, M., Gilhespy, L.A.B., Laferriere, F., Maniecka, Z., Plückthun, A., Mittl, P., et al. (2017). Functional and dynamic polymerization of the ALS-linked protein TDP-43 antagonizes its pathologic aggregation. Nat. Commun. *81*, 45. https://doi.org/10.1038/s41467-017-00062-0.

53. Kametani, F., Obi, T., Shishido, T., Akatsu, H., Murayama, S., Saito, Y., Yoshida, M., and Hasegawa, M. (2016). Mass spectrometric analysis of accumulated TDP-43 in amyotrophic lateral sclerosis brains. Sci. Rep. *61*, 23281. https://doi.org/10.1038/srep23281.

54. Dammer, E.B., Fallini, C., Gozal, Y.M., Duong, D.M., Rossoll, W., Xu, P., Lah, J.J., Levey, A.I., Peng, J., Bassell, G.J., and Seyfried, N.T. (2012). Coaggregation of RNA-binding proteins in a model of TDP-43 proteinopathy with selective RGG motif methylation and a role for RRM1 ubiquitination. PLoS One *7*, e38658. https://doi.org/10.1371/JOURNAL.PONE.0038658.

55. Coudert, L., Nonaka, T., Bernard, E., Hasegawa, M., Schaeffer, L., and Leblanc, P. (2019). Phosphorylated and aggregated TDP-43 with seeding properties are induced upon mutant Huntingtin (mHtt) polyglutamine expression in human cellular models. Cell. Mol. Life Sci. *76*, 2615–2632. https://doi.org/10.1007/S00018-019-03059-8.

56. Schwab, C., Arai, T., Hasegawa, M., Yu, S., and McGeer, P.L. (2008). Colocalization of transactivation-responsive DNA-binding protein 43 and huntingtin in inclusions of Huntington disease. J. Neuropathol. Exp. Neurol. *67*, 1159–1165. https://doi.org/10.1097/NEN.0B013E31818E8951.

57. Sassone, J., Reale, C., Dati, G., Regoni, M., Pellecchia, M.T., and Garavaglia, B. (2021). The role of VPS35 in the pathobiology of Parkinson's disease. Cell. Mol. Neurobiol. *41*, 199–227. https://doi.org/10.1007/S10571-020-00849-8.

58. Strong, M.J., Volkening, K., Hammond, R., Yang, W., Strong, W., Leystra-Lantz, C., and Shoesmith, C. (2007). TDP43 is a human low molecular weight neurofilament (hNFL) mRNA-binding protein. Mol. Cell. Neurosci. *35*, 320–327. https://doi.org/10.1016/J.MCN.2007.03.007.

59. Swarup, V., Phaneuf, D., Bareil, C., Robertson, J., Rouleau, G.A., Kriz, J., and Julien, J.P. (2011). Pathological hallmarks of amyotrophic lateral sclerosis/frontotemporal lobar degeneration in transgenic mice produced with TDP-43 genomic fragments. Brain *134*, 2610–2626. https://doi.org/10.1093/BRAIN/AWR159.

60. Yu, H., Lu, S., Gasior, K., Singh, D., Vazquez-Sanchez, S., Tapia, O., Toprani, D., Beccari, M.S., Yates, J.R., Da Cruz, S., et al. (2021). HSP70 chaperones RNA-free TDP-43 into anisotropic intranuclear liquid spherical shells. Science *371*, eabb4309. https://doi.org/10.1126/SCIENCE.ABB4309.

61. Kitamura, A., Iwasaki, N., and Kinjo, M. (2018). Molecular chaperone HSP70 prevents formation of inclusion bodies of the 25-kDa C-terminal fragment of TDP-43 by preventing aggregate accumulation. Cell Stress Chaperones *23*, 1177–1183. https://doi.org/10.1007/S12192-018-0930-1.

62. Iguchi, Y., Eid, L., Parent, M., Soucy, G., Bareil, C., Riku, Y., Kawai, K., Takagi, S., Yoshida, M., Katsuno, M., et al. (2016). Exosome secretion is a key pathway for clearance of pathological TDP-43. Brain *139*, 3187–3201. https://doi.org/10.1093/BRAIN/AWW237.

63. Zhang, N., Gu, D., Meng, M., and Gordon, M.L. (2020). TDP-43 is elevated in plasma neuronal-derived exosomes of patients with alzheimer's disease. Front. Aging Neurosci. *12*, 166. https://doi.org/10.3389/FNAGI.2020.00166.

64. Feiler, M.S., Strobel, B., Freischmidt, A., Helferich, A.M., Kappel, J., Brewer, B.M., Li, D., Thal, D.R., Walther, P., Ludolph, A.C., et al. (2015). TDP-43 is intercellularly transmitted across axon terminals. J. Cell Biol. *211*, 897–911. https://doi.org/10.1083/JCB.201504057.

65. Hopp, S.C., Lin, Y., Oakley, D., Roe, A.D., Devos, S.L., Hanlon, D., and Hyman, B.T. (2018). The role of microglia in processing and spreading of bioactive tau seeds in Alzheimer's disease. J. Neuroinflammation *15*, 1–15. https://doi.org/10.1186/S12974-018-1309-Z.

66. Li, Q., and Haney, M.S. (2020). The role of glia in protein aggregation. Neurobiol. Dis. *143*, 105015. https://doi.org/10.1016/J.NBD.2020.105015.

67. Kanlaya, R., Sintiprungrat, K., Chaiyarit, S., and Thongboonkerd, V. (2013). Macropinocytosis is the major mechanism for endocytosis of calcium oxalate crystals into renal tubular cells. Cell Biochem. Biophys. *67*, 1171–1179. https://doi.org/10.1007/S12013-013-9630-8.

68. Earls, R.H., Menees, K.B., Chung, J., Gutekunst, C.A., Lee, H.J., Hazim, M.G., Rada, B., Wood, L.B., and Lee, J.K. (2020). NK cells clear α-synuclein and the depletion of NK cells exacerbates synuclein pathology in a mouse model of α-synucleinopathy. Proc. Natl. Acad. Sci. USA *117*, 1762–1771. https://doi.org/10.1073/PNAS.1909110117.

69. Magae, J., Nagi, T., Takaku, K., Kataoka, T., Koshino, H., Uramoto, M., and Nagai, K. (1994). Screening for specific inhibitors of phagocytosis of thioglycollate-elicited macrophages. Biosci. Biotechnol. Biochem. *58*, 104–107. https://doi.org/10.1271/BBB.58.104.

70. Soldati, T., and Schliwa, M. (2006). Powering membrane traffic in endocytosis and recycling. Nat. Rev. Mol. Cell Biol. *712*, 897–908. https://doi.org/10.1038/nrm2060.

71. Bargsted, L., Medinas, D.B., Traub, F.M., Rozas, P., Muñoz, N., Nassif, M., Jerez, C., Catenaccio, A., Court, F.A., Hetz, C., et al. Disulfide cross-linked multimers of TDP-43 and spinal motoneuron loss in a TDP-43 A315T ALS/FTD mouse model. Sci. Rep. 7, 14266.10.1038/s41598-017-14399-5.

72. Riemenschneider, H., Guo, Q., Bader, J., Frottin, F., Farny, D., Kleinberger, G., Haass, C., Mann, M., Hartl, F.U., Baumeister, W., et al. (2022). Gel-like inclusions of C-terminal fragments of TDP-43 sequester stalled proteasomes in neurons. EMBO Rep. *23*, e53890. https://doi.org/10.15252/EMBR.202153890.

73. Robinson, J.L., Geser, F., Stieber, A., Umoh, M., Kwong, L.K., Van Deerlin, V.M., Lee, V.M.Y., and Trojanowski, J.Q. (2013). TDP-43 skeins show properties of amyloid in a subset of ALS cases. Acta Neuropathol. *125*, 121–131. https://doi.org/10.1007/S00401-012-1055-8.

74. Fang, Y.S., Tsai, K.J., Chang, Y.J., Kao, P., Woods, R., Kuo, P.H., Wu, C.C., Liao, J.Y., Chou, S.C., Lin, V., et al. (2014). Full-length TDP-43 forms toxic amyloid oligomers that are present in frontotemporal lobar dementia-TDP patients. Nat. Commun. *5*, 4824. https://doi.org/10.1038/ncomms5824.

75. Shaw, G., Morse, S., Ararat, M., and Graham, F.L. (2002). Preferential transformation of human neuronal cells by human adenoviruses and the origin of HEK 293 cells. FASEB J. *16*, 869–871. https://doi.org/10.1096/FJ.01-0995FJE.

76. Perez-Riverol, Y., Bai, J., Bandla, C., García-Seisdedos, D., Hewapathirana, S., Kamatchinathan, S., Kundu, D.J., Prakash, A., Frericks-Zipper, A., Eisenacher, M., et al. (2022). The PRIDE database resources in 2022: a hub for mass spectrometry-based proteomics evidences. Nucleic Acids Res. *50*, D543–D552. https://doi.org/10.1093/NAR/GKAB1038.

77. Quiroga, I.Y., Cruikshank, A.E., Bond, M.L., Reed, K.S.M., Evangelista, B.A., Tseng, J.H., Ragusa, J.V., Meeker, R.B., Won, H., Cohen, S., et al. (2022). Synthetic amyloid beta does not induce a robust transcriptional response in innate immune cell culture systems. J. Neuroinflammation *19*, 99. https://doi.org/10.1186/S12974-022-02459-1.

78. Newman, G.R., and Hobot, J.A. (1993). Resin embedding protocols for chemically fixed tissue. Resin Microsc. 47–65. https://doi.org/10.1007/978-3-642-97481-6_3.

79. Rank, L., Herring, L.E., and Braunstein, M. (2021). Evidence for the mycobacterial Mce4 transporter being a multiprotein complex. J. Bacteriol. *203*, e00685-20. https://doi.org/10.1128/JB.00685-20.

80. Tyanova, S., Temu, T., Sinitcyn, P., Carlson, A., Hein, M.Y., Geiger, T., Mann, M., and Cox, J. (2016). The Perseus computational platform for comprehensive analysis of (prote)omics data. Nat. Methods *13*, 731–740. https://doi.org/10.1038/NMETH.3901.

81. Young, M.D., Wakefield, M.J., Smyth, G.K., and Oshlack, A. (2010). Gene ontology analysis for RNA-seq: accounting for selection bias. Genome Biol. *11*, R14. https://doi.org/10.1186/GB-2010-11-2-R14.

82. Killebrew, D.A., Williams, K.S., Xie, Y., Longo, F., and Meeker, R.B. (2022). Suppression of HIV-associated macrophage activation by a p75 neurotrophin receptor ligand. J. Neuroimmune Pharmacol. *17*, 242–260. https://doi.org/10.1007/S11481-021-10002-X.

CellPress
OPEN ACCESS

STAR★METHODS

KEY RESOURCES TABLE

REAGENT or RESOURCE	SOURCE	IDENTIFIER
Antibodies		
TDP-43	Proteintech	10782-2-AP; RRID: AB_615042
TDP-43 (3H8)	Milipore Sigma	MABN45
pSer(409/410)-TDP-43 (1D3)	Milipore Sigma	MABN14; RRID: AB_11212279
Human TDP-43	Proteintech	60019-2-Ig; RRID: AB_2200520
HspA1A/B (C92F3A-5)	Enzo	ADI-SPA-810; RRID: AB_10616513
GFP	Novus Biological	NB100-1614; RRID: AB_10001164
1039C	Gift from CNDR, Philadelphia PA	N/A
Biotinylated TDP-43 (3H8)	Novus	NBP1-92695; RRID: AB_11005586
Goat anti-Mouse IgG (H+L) Secondary Antibody, HRP	Invitrogen	31430
Donkey anti-Rabbit IgG (H+L) Cross-Adsorbed Secondary Antibody, HRP	Invitrogen	31458
Goat anti-Chicken IgY (H+L) Secondary Antibody, HRP	Invitrogen	A16054
Goat anti-Rat IgG (H+L) Secondary Antibody, HRP	Invitrogen	31470
12 nm Colloidal Gold AffiniPure Goat Anti-Mouse IgG (H+L)	Jackson Immuno	115-205-166
Pierce High Sensitivity Streptavidin-HRP	Thermo Scientific	21130
Goat anti-Chicken IgY (H+L) Secondary Antibody, Alexa Fluor™ 488	Invitrogen	A-11039
Goat anti-Mouse (H+L) Secondary Antibody, Alexa Fluor™ 647	Invitrogen	A-21235
Biological samples		
Control 1 motor cortex	VA Biorepository	100036
Control 2 motor cortex	VA Biorepository	110001
ALS 1 motor cortex	VA Biorepository	AZ190033
ALS 2 motor cortex	VA Biorepository	AZ200012
Chemicals, peptides, and recombinant proteins		
Intercept (TBS) Blocking Buffer	Licor Biosciences	927-60001
Bissulfosuccinimidyl suberate (BS3)	Thermo Scientific	21580
RQ1 DNase I	Promega	M6101
Proteinase K	Millipore Sigma	P6556
Pierce Gentle Ag/Ab Elution Buffer, pH 6.6	Thermo Scientific	21013
rhGM-CSF	R&D Systems	215-GM-010/CF
Acti-stain 555 phalloidin	Cytoskeleton Inc.	PHDH1
CellTracker Red CMTPX	Invitrogen	C34552
DAPI	ThermoFisher	D1306
Cytochalasin D	Sigma	C2873
Dimethyl sulfoxide	Sigma	D2650
Wheat-germ agglutinin Alexa-fluor 647	ThermoFisher	W32466
Deposited data		
TDiP Proteome	ProteomeXchange Consortium	PXD035705

(*Continued on next page*)

Continued

REAGENT or RESOURCE	SOURCE	IDENTIFIER
Experimental models: Cell lines		
HEK293A	ThermoFisher	R70507
Experimental models: Organisms/strains		
C57Bl/6	Charles River	Strain Code: 027
Oligonucleotides		
TDP-43-F 5′-gctcaagctttaatgtctgaatatattcgggtaacc	This paper	N/A
TDP-43-R 5′-cggtggatcctacattccccagccaga	This paper	N/A
410SA-C1-F 5′-gccggctggggaatgtaggatc	This paper	N/A
409SA-R 5′-ggccttagaatccatgcttgagcc	This paper	N/A
mCherry-F 5′- tccaccggtcgccaccatggtgagcaagggcgaggag	This paper	N/A
mCherry-R 5′-ccttgtacagctcgtccatgccgcc	This paper	N/A
Recombinant DNA		
pcDNA-5TO-GFP-TDP-43-ΔNLS-K192Q	Cohen et al.[17]	N/A
pcDNA-5TO-GFP-TDP-43-ΔNLS-K192Q-S409/410A	This paper	N/A
pcDNA3.1-mCherry	This paper	N/A
Software and algorithms		
Prism Version 9	GraphPad Software	https://www.graphpad.com/features
ImageJ	Schneider et al.	https://imagej.nih.gov/ij/
Zen	Zeiss	https://www.zeiss.com/microscopy/en/products/software/zeiss-zen.html
Proteome Discoverer	Thermo Scientific	https://www.thermofisher.com/us/en/home/industrial/mass-spectrometry/liquid-chromatography-mass-spectrometry-lc-ms/lc-ms-software.html
Perseus	MaxQuant	https://maxquant.net/perseus/
Ingenuity Pathway Analysis	Qiagen	https://digitalinsights.qiagen.com/products-overview/discovery-insights-portfolio/analysis-and-visualization/qiagen-ipa/
Other		
Trypsin	Promega	25200-056
Dulbecco's Modified Eagle Media (DMEM),	Gibco	31-053-028
Fetal bovine serum (FBS)	Sigma	F2442
L-glutamine	Gibco	25030-081
FuGENE 6 Transfection Reagent	Promega	E2691
Protein A/G magnetic agarose	Thermo Scientific	78609
ProteoJuice Protein Transfection Reagent	Millipore Sigma	71281
Penicillin/Streptomycin	Thermo Scientific	15140-122

RESOURCE AVAILABILITY

Lead contact

Further information and any associated requests should be made to the lead contact, Todd Cohen (toddcohen@neurology.unc.edu).

Materials availability

This study did not generate new unique reagents. Pertinent experimental materials are listed in the key resources table and individual STAR Methods sections.

Data and code availability

All data generated and analyzed in this study are included in this study and can be obtained from the authors upon reasonable request. The mass spectrometry proteomics data have been deposited to the ProteomeXchange Consortium via the PRIDE[76] partner repository with the dataset identifier Database: PXD035705. Please direct all requests to Todd Cohen (toddcohen@neurology.unc.edu).

EXPERIMENTAL MODEL AND SUBJECT DETAILS

Human ALS and control brain specimens from male donors (Table S1) were provided by the Department of Veterans Affairs Biorepository under approved VA Merit review BX002466. Human peripheral blood mononuclear cells were isolated from de-identified human donor blood (equal ratios of males and females) through the New York Blood Center. Primary microglia were isolated from equal ratios of male and female C57Bl/6 mice (Charles River) in strict compliance with animal protocols approved by the Institutional Animal Care and Use Committee (IACUC) of the University of North Carolina at Chapel Hill (protocol #21.257). The authors have not observed any influence of sex on the results of this study. Cultured HEK293A cells were confirmed to be negative for mycoplasma contamination.

METHOD DETAILS

Plasmid construction

The following plasmids were generated for use in this study: pTX066 (GFP-TDP43-ΔNLS-K145Q), pTX128 (GFP-TDP43- ΔNLS-K145Q-2SA containing S409/410A mutations), and pTX428 (mCherry-P2A-T2A). To generate pTX066, PCR cloning was used amplify a HindIII/BamHI fragment from the original myc-tagged TDP43-ΔNLS-K145Q plasmid that we previously reported,[17] and this fragment was inserted into the pEGFP-C1 expression plasmid. To generate pTX128, we used pTX066 as a template, and 410SA-C1-F/409SA-R primers were used to amplify and introduce mutations to add S409/410A into the GFP-TDP43-mNLS-K145Q vector. Following fragment purification, ligation reactions were performed containing T4 polynucleotide kinase, DpnI and T4 DNA ligase at room temperature for 1 hr, and the ligation product was transformed into DH5a competent cells. pTX428 (pcDNA3.1 mCherry-P2A-T2A) was generated by replacing the eGFP casette in pcDNA3.1 eGFP-P2A-T2A. To accomplish this, mCherry was amplified using mCherry-F and mCherry-R primers, and the DNA fragment was purified and inserted into pcDNA3.1 eGFP-P2A-T2A using AgeI and BsrGI restriction enzymes. PCR primer sequences used in this study were as follows. For PCR cloning, TDP-43-F (gctcaagctttaatgtctgaatatattcgggtaacc) and TDP-43-R (cggtggatcctacattccccagccaga) were used. For mutagenesis, 410SA-C1-F (gccggctggggaatgtaggatc) and 409SA-R (ggccttagaatccatgcttgagcc) were used. For imaging studies, mCherry-F (tccaccggtcgccaccatggtgagcaagggcgaggag) and mCherry-R (ccttgtacagctcgtccatgccgcc) were used.

Cell culture and transfection

HEK293A cells (ThermoFisher #R70507) were cultured in Dulbecco's Modified Eagle Media (DMEM, Gibco) supplemented with 10% fetal bovine serum (Sigma) and 100 mM L-glutamine (Gibco) and incubated at 37°C under 5% CO_2. This subclone of the standard HEK293 cell line was chosen due to its slower growth rate and ability to maintain ectopic expression of plasmids during mitotic events. Cells were transfected with pcDNA-5TO-GFP-TDP-43-ΔNLS-K192Q, pcDNA-5TO-GFP-TDP-43-ΔNLS-K192Q-S409/410A, or pcDNA3.1-mCherry as indicated, using Fugene 6 transfection reagent (Promega #E269A) according to manufacturer instructions. Cells were rinsed in 1X cold PBS 48-hour post-transfection and harvested in 1.0 mL radioimmunoprecipitation assay buffer (RIPA) with protease, phosphatase, and deacetylase inhibitors (PMSF, NCA, TSA, PIC, sodium orthovanadate, beta-glycerophosphate, and sodium fluoride). Lysates were stored at −80°C until further processing.

Primary macrophage culture

Macrophages were cultured from human peripheral blood mononuclear cells as previously described.[77] Briefly, human Leukopaks (New York Blood Center) were overlayed atop a ficoll-hypaque density gradient and centrifuged at 120 RCF for 20 minutes. The buffy coat was isolated using a Pasteur pipette and washed in 1X PBS and centrifuged as above. The pellet was resuspended in erythrocyte lysis buffer (155 mM NH_4Cl, 10 mM $KHCO_3$, and 0.1 mM EDTA) and gently agitated for 10 minutes at room temperature. Cells were rinsed 2 additional times as above. Viability and cell counts were obtained via trypan blue exclusion and hemocytometry method. Cells were maintained in DMEM supplemented with 10% fetal bovine serum. Monocytes were allowed to differentiate into macrophages for 5 days in the presence of 15 ng/ml human

granulocyte–macrophage colony stimulating factor (rhGM-CSF; R&D Systems # 215-GM-010/CF). Non-adherent cells were aspirated and differentiated macrophages were maintained with half-media changes every other day at 37°C, 5% CO_2.

Tandem detergent-extraction and immunoprecipitation of proteinopathy (TDiP)

Bead preparation

30 μL of resuspended Pierce protein A/G magnetic agarose (Thermo Scientific #78609) were washed 3X in dilution buffer (150 mM Tris 7.4, 100 mM NaCl, 10 mM EDTA), transferred to 1.0 mL of RIPA buffer with 15 μg ProteinTech 10782-2-AP, and incubated for 2 hours at 4°C with constant rotation. For optional crosslinking: beads were then washed 3X in 0.1% TBS-T (20 mM Tris, 150 mM NaCl, 0.1% Tween-20), then 2X in PBS, before resuspension in 5 mM BS3 crosslinker in PBS (Thermo Scientific #21580). Crosslinking occurred for 30 minutes at room temperature with constant rotation, followed by quenching for 15 minutes with 1:10 of 1M Tris-HCl, pH 7.5. Non-crosslinked immunoglobulins were stripped by washing beads 3X in 1 mL Gentle Ab elution buffer (Thermo Scientific #21013). Beads were washed again 3x in TBS-T and then blocked overnight in Intercept TBS non-protein-based blocking buffer (Licor Biosciences #927-60001) with 1 mM DTT and 1% Tween-20 under constant rotation.

Cell lysate preparation

Lysates containing ΔNLS-K145Q insoluble aggregates were thawed on ice followed by successive rounds of syringe-based lysis using progressively larger gage syringe (18g→21g→25g). Lysates were then supplemented with 10X RQ1 DNAseI buffer (Promega #M6101) to achieve a final concentration of 1X. DNAseI was added to a final concentration of 50 units/mL then incubated at 37°C for 30 minutes with intermittent inversion. Note, excessive force denatures DNAse I, thus in contrast to benzonase-based extraction methods, we did not vortex the sample until after the addition of sarkosyl to afinal concentration of 0.5%. Lysates were then vortexed vigorously for 30 seconds at top speed, and then re-lysed using the syringe strategy above. The lysate should appear clear of any genomic DNA or membrane fragments. The lysate was then filtered through a 0.45 μm filter syringe pre-wet with 1X RIPA buffer. Lysates were centrifuged at 100,000 RCF for 1 hour at 4°C. The supernatant was removed, and the pellet was reconstituted in extraction buffer (1X RIPA, 1% Tween-20, 0.5% Sarkosyl, 1 mM DTT) and sonicated 20 times with 1-second pulses on ice using a QSonica Q125 hand sonicator probe.

Human tissue lysate preparation for TDiP analysis

ALS and non-neurological control brain specimens were provided by the Department of Veterans Affairs (VA) Biorepository under VA merit review BX002466. Posterior frontal cortex was pulverized into a fine powder using the Cryo-Cup and pestle tissue homogenizer (Research Products International, #141420) that was pre-cooled with liquid nitrogen. Tissue powder was aliquoted in 100mg aliquots then snap-frozen on dry ice. Tissue powder was lysed and filtered as above. Following filtration, lysates were pre-cleared at 18,000 RCF for 30 min at 4°C to remove tissue debris and most contaminating myelin (note, this pellet can be cleaned by sonication in RIPA + 35% sucrose and an additional centrifugation step for further characterization). The remaining supernatant was gently overlayed atop a 1X RIPA + 35% sucrose cushion using a 25-gage syringe, then centrifuged at 100,000 RCF for 1 hour at 4°C. This supernatant was then collected as the soluble fraction. The intermediate phase consisting of lipids was discarded along with the lower sucrose phase. The pellet was washed 1X in lysis solution, vortexed for 30 seconds at top speed, then centrifuged again at 100,000 RCF for 30 minutes. The pellet was finally sonicated in extraction buffer as above.

Immunoprecipitation and elution

The total bead slurry was combined with homogenate and allowed to bind for an additional 16 hours. Supernatants were removed and beads washed 3X in washing buffer (1X RIPA, 0.5% Sarkosyl, 1 mM DTT, 1% Tween-20). Protein complexes were eluted using 5 M NaCl at 56°C for 15 minutes. Elution products were spun at 100,000 RCF for 30 minutes at 4°C, then washed in 1X PBS. To prepare for use, pellets were reconstituted in 1X PBS followed by 4 cycles of 20, 1-second pulses.

Considerations when using the TDiP protocol

The choice of antibody can be tailored based on the user end-goal provided that the antigen interactions are not destabilized by the harsh buffers, which can be determined empirically. For example, we noted this caveat when purifying TDP-43 aggregates with a Chromotek nanobody, GFP-trap magnetic agarose

(#gta-10) instead of 10782-2-AP or 3H8. In this scenario, we found that the nanobody was destabilized by the 1% Tween-20-containing extraction buffer and resulted in virtually no yield (*not shown*) despite the nanobody's reported high-affinity paratope-epitope interaction (K_D = 1 pM).

Immunoblotting

Unless otherwise indicated, samples were denatured in 1X Laemmli buffer with or without 50 mM DTT and electrophoresed on continuous 4–20% acrylamide gel (BioRad #3450034). Proteins were transferred to 0.2 μm nitrocellulose membrane and blocked in 2% non-fat milk-TBS. All membranes were incubated with respective primary antibodies at 4°C overnight with continuous rocking. Antibodies used were as follows: TDP-43 3H8 (Millipore Sigma #MABN45), pSer(409/410)-TDP-43 1D3 (Millipore Sigma #MABN14), HSPA1A/B C92F3A-5 (Enzo # ADI-SPA-810), GFP (Novus #NB100-1614). Membranes were washed 3X with TBS-0.01% Tween 20 and incubated with HRP conjugated secondaries or streptavidin-HRP from Invitrogen as follows: anti-Mouse (#31430, 1:1000) anti-Rabbit (#31458, 1:1000) anti-Chicken (#A16054, 1:4000) and anti-Rat (#31470, 1:1000) for 1 hour at room temperature followed by an additional 3 washes and development via enhanced chemiluminescence. High-sensitivity Streptavidin HRP (#21130, 1:8000) was incubated for 15 minutes at room temperature followed by five, 15-minute washes in TBS-T. A detailed list of all primary antibodies is shown in Table S3, and all secondary antibodies are shown in Table S4.

Limiting proteinase resistance assay

Proteinase K (Millipore Sigma #P6556) was diluted serially from 2.5 μg/mL to 0.039 μg/mL in 1X PBS. 2 μL of washed bead slurry containing insoluble aggregated TDP-43 (ΔNLS-K145Q) was added to each tube and incubated for 30 minutes at 37°C with intermittent mixing. The reaction was quenched with 10 mM PMSF and boiled at 98°C in the presence of non-reducing 1x Laemmli buffer. Samples were spun at 10,000 RCF for 5 minutes and loaded onto continuous 4–20% gradient SDS-PAGE.

Negative stain and immunogold electron microscopy

This approach was adapted from Geoffrey et al., 1993.[78] Following elution, aggregates were centrifuged at 100,000 RCF for 30 minutes. The pellet was rinsed of salts by sonicating as above in 0.5 mL double deionized water. This rinsed was repeated once. Aggregates were sonicated once more in 200 μL water (adjusted to a final concentration of 100 μg/mL by A280 absorbance readings). Protein aliquots were fixed for 1 hour at room temperature in 2.5% glutaraldehyde in 0.15M sodium phosphate buffered and immediately processed for negative stain immuno-electron microscopy in a humidified chamber. A glow-discharged formvar/carbon-coated 400 mesh copper grids (Ted Pella, Inc., Redding, CA) was floated on a 20 μL droplet of the fixed sample suspension for 3 minutes. Grids were washed in blocking buffer (0.15% glycine, 0.2% BSA-Ac in 0.15 M sodium phosphate buffer) three times followed by three rinses in 0.15M sodium phosphate buffer and an additional 5-minute wash in 0.2% BSA-Ac, 0.15M sodium phosphate buffer. Grids were stained for 20 minutes with 1:50 dilution of mouse anti-human TDP-43 (Proteintech 60019-2-Ig, Rosemont IL). Unbound primary antibody was washed, using three washes followed by a 5-minute wash in 0.2% BSA-Ac, 0.15M sodium phosphate buffer. The grids were incubated for 20-minutes in a 1:20 dilution of 12 nm colloidal gold-AffiniPure goat anti-mouse IgG (H+L) secondary antibody (Jackson Immuno, Lot #151193) in 0.2% BSA-Ac in 0.15M sodium phosphate buffer. After four washes in 0.2% BSA-Ac, 0.15M sodium phosphate buffer, and two washes in 0.15M sodium phosphate buffer, grids were post-fixed for 30 seconds in 0.1% glutaraldehyde in 0.15M sodium phosphate buffer followed by four washes in deionized water for 20 seconds each. The grids were then stained with 1% aqueous uranyl acetate for 1-minute for additional contrast. Samples were observed using a JEOL JEM-1230 transmission electron microscope operating at 80 kV (JEOL USA INC., Peabody, MA) and images were taken using a Gatan Orius SC1000 CCD camera with Gatan Microscopy Suite version 3.10.1002.0 software (Gatan, Inc., Pleasanton, CA).

Proteomics analysis

Sample preparation for affinity purification mass spectrometry analysis (AP-MS)

Immunoprecipitated samples (N = 3) were rinsed in 100 mM Tris-HCl (pH 7.8), three times, and were subjected to on-bead trypsin digestion, as previously described.[79] 50 μL of 50 mM ammonium bicarbonate (pH 8) containing 1 μg trypsin (Promega) was added to beads overnight at 37°C with shaking. The next day, 500 ng of trypsin was added then incubated for an additional 3 h at 37°C with shaking. Supernatants from pelleted beads were transferred, then beads were washed twice with 50 μL LC/MS grade water. These

rinses were combined with original supernatant, then acidified to 2% formic acid. Peptides were desalted with peptide desalting spin columns (Thermo) and dried via vacuum centrifugation. Peptide samples were stored at −80°C until further analysis.

LC/MS/MS analysis

Each sample was analyzed by liquid chromatography tandem mass spectrometry (LC-MS/MS) using an Easy nLC 1200 coupled to a QExactive HF (Thermo Scientific). Samples were injected onto an Easy Spray PepMap C18 column (75 μm id × 25 cm, 2 μm particle size) (Thermo Scientific) and separated over a 120 min method. The gradient for separation consisted of a step gradient from 5 to 35 to 45% mobile phase B at a 250 nl/min flow rate, where mobile phase A was 0.1% formic acid in water and mobile phase B consisted of 0.1% formic acid in acetonitrile (ACN). The QExactive HF was operated in data-dependent mode where the 15 most intense precursors were selected for subsequent HCD fragmentation. Resolution for the precursor scan (m/z 300–1600) was set to 120,000 with a target value of 3×10^6 ions, 100 ms inject time. MS/MS scans resolution was set to 15,000 with a target value of 1×10^5 ions, 75 ms inject time. The normalized collision energy was set to 27% for higher-energy C-trap dissociation (HCD), with an isolation window of 1.6 m/z. Peptide match was set to preferred, and precursors with unknown charge or a charge state of 1 and ≥ 8 were excluded. All peptides identified by LC/MS/MS are listed in Table S1.

Data analysis

Raw data files were processed using Proteome Discoverer 2.5 and searched against the reviewed human database (containing 20245 sequences), appended with the mutant TARDBP sequence, using Sequest. Tryptic peptides were identified using the following parameters: minimum peptide length was set to 5 and up to two missed cleavage sites were allowed. Variable modifications included: oxidation of M, phosphorylation of S/T/Y, GlyGly of K, and acetyl of K. Label-free quantification (LFQ) using razor + unique peptides was enabled. A 1% false discovery rate (FDR) was used to filter proteins and peptides. A minimum of two peptides per protein and <50% missing values across all samples was required for further analysis.

Normalized data were exported from Proteome Discoverer and imported into Perseus version 1.6.14.0 [80] for additional analysis. Imputation of missing values based on normal distribution with width of 0.3 and downshift of 1.8, was performed. Student's t-test was performed for each pairwise comparison (TDP_Isotype) and FDR corrected q-value and p value were calculated. A log2 fold change ratio for TDP_Isotype was calculated using the normalized quantitative values and a log2 ratio ±-1 was considered significant. Perseus was used to generate figures. Ingenuity Pathway Analysis (IPA; Qiagen) was used for pathway analysis. Enrichment analysis was performed using Goana Gene Ontology and KEGG Pathway Analysis package in R.[81]

Immunofluorescence

HEK293 cells were seeded to PDL-coated coverslips (Neuvitro #GG12PDL) such that they reached 50% confluency on day of transfection. Cells were transfected with 500 ng of pTX066 or pEGFP-C1 using Fugene 6 transfection reagent per manufacturer protocol. Forty-eight hours post-transfection, cells were fixed in 4% paraformaldehyde (EMS, Hatfield PA) for 10 minutes at room temperature followed by washing in 1X PBS and permeabilization in 0.2% Triton X-100/PBS for 8 minutes. Cells were rinsed in PBS and blocked in 2.0% non-fat milk made up in 0.2% TBS-T for 1 hour at room temperature. Cells were incubated with HSPA1A/B C92F3A-5 (1:500) in blocking buffer for 16 hours at 4°C. Cells were washed 3X in TBS-T and incubated with Alexa-fluor 647-conjugated anti-mouse secondary antibody (Invitrogen # A-28181, 1:500) for 1 hour at room temperature and counterstained with 100 nM DAPI in PBS. Coverslips were mounted with ProLong Diamond Antifade mountanti (Invitrogen, #P36961).

Confocal microscopy

Images were obtained on an inverted Zeiss 800/Airyscan laser scanning confocal microscope fitted with 405, 488, 561, and 647 nm diode lasers and gallium arsenide phosphide (GaAsP) detectors. All image acquisition used a 63X oil-immersion lens. Orthogonal projections in Figures 4A and 4B were generated in ZEN blue software (Version 3.1; Carl Zeiss Microscopy) and image brightness/contrast adjusted in Adobe Photoshop. Orthogonal and maximum intensity projections in Figure 4C were generated using ImageJ (NIH).

Live-cell HEK293 protein transduction assay

HEK293 cells were seeded to 8-chamber dishes (Cellvis #C8-1.5H-N) such that they reached 50% confluence 16 hours post-seeding. Cells were transfected with a control mCherry expression vector made in-house (pcDNA3.1-P2A-mCherry-T2A) using Fugene 6 Transfection reagent according to manufacturer protocol. 24 hours later, 10.0 μg (A_{280}) of TDiP aggregates per well (~80 mm^2), were transfected into cells using ProteoJuice Transfection reagent (Millipore Sigma #71281). Ratios were adapted for chamber dish from manufacturer protocol and De Rossi et al., 2021. 4 hours following transfection, cells were returned to complete media and imaged on a 37°C heated stage in a humidified, 5% CO_2 chamber.

Live-cell microglia phagocytosis assay

All mouse procedures were performed in strict compliance with animal protocols approved by the Institutional Animal Care and Use Committee (IACUC) of the University of North Carolina at Chapel Hill (#21.257). Primary mouse microglia were cultured as previously described.[82] Briefly, cortical structures from embryonic day 18 mice were gently fragmented with a 21-gage blunt syringe. Fragments were placed into a 6-well plastic, ultra-low adhesion plate in DMEM with 10% FBS and 1x penicillin/streptomycin. Approximately 7 days post plating microglia extravasate from the cortical debris and adhere to the culture substrate. Cells were washed, dissociated with 0.05% Trypsin EDTA, and plated on PDL-coated 8-chamber slides. For the assay setup, microglia were labeled with CellTracker Red CMTPX dye (Invitrogen #C34552) for 30 minutes following manufacturer instructions. Cells were then washed and replaced with complete media supplemented with TDiP aggregates at a final concentration of 10 μg/mL. Cells were immediately imaged 30-minutes post aggregate-treatment as above. A detailed list of all materials and reagents used for protein transduction, molecular, and cellular assays in this study is provided as Table S5.

Live-cell human macrophage phagocytosis assay

Differentiated macrophages were sub-cultured to 8-chamber dishes at a density of 45,000 cells per well. The next day, cells were treated with 10 μM Cytochalasin D (CD; Sigma #C2873) or vehicle control (DMSO; Sigma #D2650) at 37°C, 5.0% CO_2 for 30 minutes. DMSO concentrations never exceeded 0.1% in all conditions. Cells were treated with TDiP aggregates at a concentration of 10 μg/mL for 30 minutes in complete media, maintaining a 10 μM concentration of CD. During incubation, wheat germ agglutinin conjugated to Alexa-fluor 647 (WGA-647; ThermoFisher #W32466) was diluted to 5 μg/mL in sterile phosphate buffered saline. Cells were rinsed three times in phosphate buffered saline and incubated with WGA-647 solution for 10 minutes at 37°C to label the plasma membrane. Cells were rinsed an additional two times as above then returned to complete media containing CD or vehicle as above. Cells were immediately imaged. Internalization frequency was determined by calculating the percentage of aggregate-containing cells per randomized field of view in a blinded manner. Aggregate containment was defined as continuous containment of aggregate GFP-fluorescence signal by the WGA-647 signal.

QUANTIFICATION AND STATISTICAL ANALYSIS

Detailed descriptions of statistical methods are provided in STAR Methods under the following sections: Proteomics analysis and Live-cell human macrophage phagocytosis assay. Immunoblot densitometry was performed using Image Studio Lite for Windows (LI-COR Biosciences, Lincoln, NE). These analyses were performed using Graphpad Prism Version 9 for Windows (San Diego, CA). Data distributions were assessed for normality using the Shapiro-Wilk test. Student's parametric two-tailed t-test or ANOVA with Bonferroni correction, where appropriate, were used for column-based analyses. The alpha cutoffs for statistical significance were defined as follows: *$p < 0.05$, **$p < 0.01$, ***$p < 0.001$, and ****$p < 0.0001$.